nature protocols

https://doi.org/10.1038/s41596-024-01122-8

Protocol

Check for updates

Measuring plasma membrane fluidity using confocal microscopy

Pablo Carravilla[1,5], Luca Andronico[1,5], Jan Schlegel[1,5], Yagmur B. Urem[1], Ellen Sjule[1], Franziska Ragaller[1], Florian Weber[1,2], Cenk O. Gurdap[1], Yavuz Ascioglu[1], Taras Sych[1], Joseph Lorent[3,4] & Erdinc Sezgin[1]

Abstract

Membrane fluidity is a crucial parameter for cellular physiology. Recent evidence suggests that fluidity varies between cell types and states and in diseases. As membrane fluidity has gradually become an important consideration in cell biology and biomedicine, it is essential to have reliable and quantitative ways to measure it in cells. In the last decade, there has been significant progress both in chemical probes and in imaging tools to make membrane fluidity measurements easier and more reliable. We have recently established a robust pipeline, using confocal imaging and new environment-sensitive probes, which has been successfully used for several studies. Here we present our detailed protocol for membrane fluidity measurement from labeling to imaging and image analysis. The protocol takes ~4 h and requires basic expertise in cell culture, wet lab and microscopy.

Key points

- This protocol describes a robust pipeline for measuring plasma membrane fluidity using confocal imaging and new environment-sensitive probes. Detailed steps cover the labeling and imaging of cells and the subsequent image analysis.
- Compared with other methods for measuring membrane fluidity, this approach is easy to implement, as it can be performed with confocal microscopes and does not require a sophisticated data analysis pipeline.

Key references

Sezgin, E. et al. *Chemphyschem* **16**(7), 1387–94 (2015): https://doi.org/10.1002/cphc.201402794

Ragaller, F. et al. *Open Biol.* **12**(9), 220175 (2022): https://doi.org/10.1098/rsob.220175

Cikes, D. et al. *Nat Metab.* **5**(3), 495–515 (2023): https://doi.org/10.1038/s42255-023-00766-2

Leng, H. et al. *Nat Commun.* **13**(1), 7868 (2022): https://doi.org/10.1038/s41467-022-35358-3

Matias, MI. et al. *Cell Rep.* **37**(5), 109911 (2021): https://doi.org/10.1016/j.celrep.2021.109911

[1]Science for Life Laboratory, Department of Women's and Children's Health, Karolinska Institutet, Solna, Sweden. [2]Upper Austria University of Applied Sciences, Department Medical Engineering, Linz, Austria. [3]Membrane Biochemistry and Biophysics, Bijvoet Center for Biomolecular Research, Department of Chemistry, Utrecht University, Utrecht, the Netherlands. [4]Cellular and Molecular Pharmacology, Translational Research from Experimental and Clinical Pharmacology to Treatment Optimization, Louvain Drug Research Institute, UCLouvain, Brussels, Belgium. [5]These authors contributed equally: Pablo Carravilla, Luca Andronico, Jan Schlegel. e-mail: erdinc.sezgin@ki.se

Introduction

Besides the barrier function between the different compartments, cellular membranes are involved in multiple cellular processes such as cell signaling, endocytosis and exocytosis, intracellular trafficking, cell migration and cell division[1,2]. They are highly complex, consisting of lipids, glycolipids, membrane-associated proteins, glycoproteins and proteoglycans[3]. Hundreds of structurally diverse lipids[4] are asymmetrically distributed across and within the bilayer leaflets[5]. Collective biophysical properties of the plasma membrane such as membrane thickness, mobility, order, fluidity, polarity, tension, curvature or phase transition are highly intertwined and can be largely attributed to the lipid species present in the membrane[5–7]. For example, saturated lipids decrease membrane fluidity, while mono- and polyunsaturated lipids increase it, and cholesterol is an adaptive modulator of membrane fluidity[6,7]. Remodeling of membrane fluidity occurs as a result of alterations in the cell lipidome, and it has been linked to many physiological processes. For instance, changes in membrane fluidity accompany cell proliferation[8,9] and differentiation[10,11], and it can affect the overall mobility of migratory cells[12,13] and promote/inhibit activity of immune cells[14–16]. If lipid homeostasis is disrupted, so is the fluidity of cellular membranes, which has been associated with tumor progression[17,18] and neurodegenerative and cardiovascular diseases[19,20].

Given the role of membrane fluidity in multiple cellular processes, the interest in measuring it has increased within the last decades. Therefore, multiple fluorescent probes, so called environment-sensitive probes, have been developed and characterized[21]. Depending on their immediate environment, these probes exhibit a change in fluorescence intensity, emission wavelength or lifetime that can be measured by advanced microscopy tools. Different environment-sensitive probes can sense different membrane biophysical properties such as order, viscosity and tension, among others[22]. For membrane fluidity measurements, solvatochromic probes have become particularly popular and can distinguish disordered membranes (unsaturated lipids) from ordered membranes (saturated lipids) by a red shift in the emission wavelength[21].

Here, it is critical to clarify the use of the term ‘fluidity’. Membrane fluidity, order and lipid packing are often used interchangeably in literature. Indeed, such biophysical parameters are closely linked in membranes and are challenging to dissect experimentally. We consider fluidity as an overarching parameter of cellular membranes that can be measured via multiple means, which will be discussed later. Here, we focus on the spectral shift of solvatochromic probes, which give quantitative insights on membrane fluidity by measuring membrane order. The underlying mechanism of the emission shift for these probes is solvent relaxation: with more molecules (that is, water molecules in biological systems) in the solvation envelope of the fluorophore, the system can relax resulting in decreased energy of the excited state, hence the probe exhibits a red shift[23]. Multiple features of the membrane can affect solvent relaxation, such as acyl chain saturation of lipids and cholesterol content. Depending on such parameters, the membrane can be more ‘ordered’ or ‘disordered’. Disordered membranes are loosely packed and more hydrated, which is why solvatochromic probes are subjected to more solvent relaxation and their emission spectra are red shifted[24]. The spectral shift of the probes is often examined using spectral or two-channel/ratiometric imaging and subsequent quantification by calculation of intensity ratios or the generalized polarization (GP) parameter. An increase in disorder within the membrane environment experienced by environment sensitive probes causes the probe to exhibit a shift toward longer wavelengths leading to lower intensity ratios (GP values)[25,26]. Generally, a more disordered environment is more fluid, as experienced by these probes; however, the absolute GP values are highly dependent on the probe and imaging system. Technical details of the GP measurements and the strengths of this approach are described herein. Limitations to this approach are also considered in the ‘Limitations’ section.

Development of the protocol

Historically, two-photon microscopy was used with the solvatochromic probe Laurdan, and two channel emissions were collected using beam splitters and two detectors[27]. Membrane fluidity

is usually quantified via the GP parameter, which is calculated according to equation (1) using the two channels. I_o (ordered channel intensity) and I_d (disordered channel intensity) refer to the fluorescence intensity measured from the channel centered at the left-hand or right-hand side of the emission spectrum, respectively,

$$GP = \frac{I_o - I_d}{I_o + I_d}. \quad (1)$$

Based on its definition, GP can vary from −1 (low order) to +1 (high order), and it does not depend on absolute intensity values but rather on the spectral shift of the fluorescent probe. The GP values obtained for the same sample but with different instruments, detectors and settings might show variations as these parameters change the intensity values measured at different wavelengths. Therefore, it is important to note that the GP value obtained with equation (1) is an empirical parameter. To account for differences between different instrument settings, detector settings and sensitivities, a calibration factor (G) can be used[28]. The G factor is often obtained by measuring the environment-sensitive probe in a solvent such as dimethyl sulfoxide (DMSO). Alternatively, a reference membrane can be used before every measurement, and the data can be presented as ΔGP (that is, $GP_{sample} - GP_{reference}$)[29].

Subsequently, two-channel confocal imaging in combination with environment-sensitive probes has been used to measure the GP parameter[30,31]. The availability of confocal microscopes, as well as probes in the visible spectrum have increased the applicability of these measurements. Recently, spectral confocal microscopy has permitted the recording of the full emission spectrum of probes, by dispersing the emitted light onto an array of detectors (Fig. 1). We and others exploited this over the last years to measure the full spectrum of the probe in cellular membranes. Compared with the two-channel mode, spectral imaging allows to select the best combination of wavelengths (that is, position and width of emission windows) to improve both signal-to-noise and GP resolution[26,32]. Here, we present our protocol for measuring membrane fluidity using two-channel and spectral confocal imaging with newly developed environment sensitive probes.

Application of the method

Two-color or spectral imaging in combination with environment-sensitive probes has been used to study various aspects of cell biology including membrane asymmetry[33,34] (Box 1), apoptosis[35], protein mobility[36,37], endocytosis and maturation of endosomes[38–40], voltage sensing in neurons[41], segregation of GPI-anchored proteins[42], lipid transfer from lipoproteins

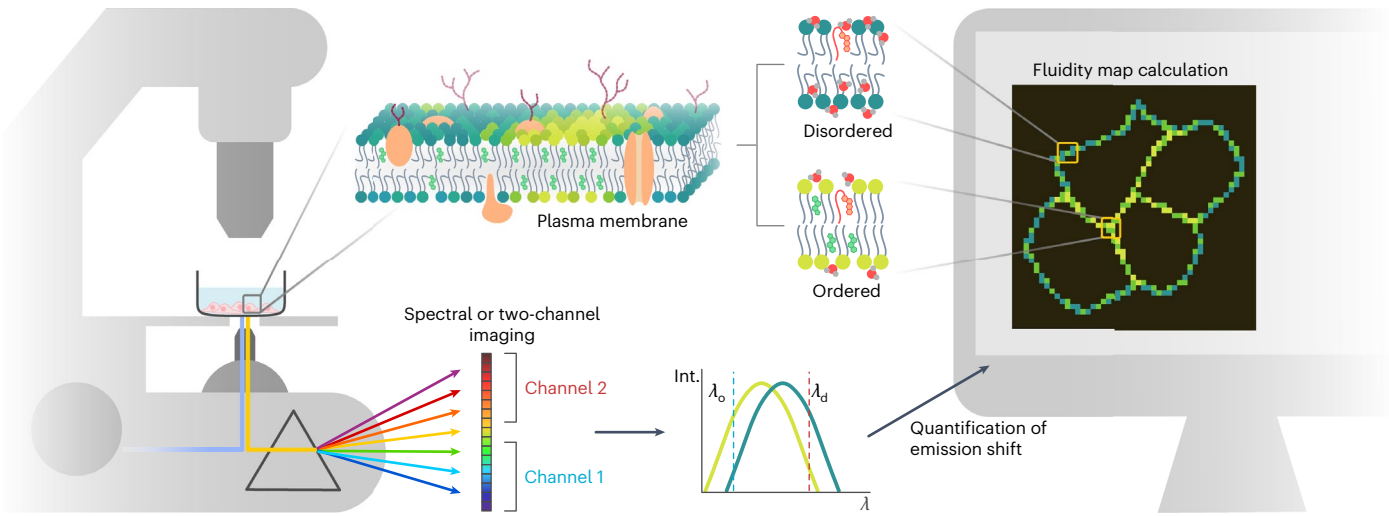

Fig. 1 | Ratiometric imaging with two-channel or spectral confocal microscopy to measure membrane fluidity. Eukaryotic plasma membranes are heterogeneous in lipid composition, which can give rise to distinct membrane fluidity. This can be quantified using environment-sensitive dyes and spectral or two-channel confocal imaging.

BOX 1

Membrane fluidity and membrane asymmetry

Lipidomic analysis revealed that the cytoplasmic cell membrane leaflet contains twice as many acyl chain unsaturations than the exoplasmic leaflet. A consequence of this compositional asymmetry is fluidity asymmetry, with the outer leaflet being highly ordered and the inner monolayer displaying lower ordering[5,91]. The reasons for a cell to spend a significant amount of energy to produce an asymmetrically packed cell membrane could be diverse. A highly packed and rigid outer leaflet should provide resistance toward physical stress and intrusion of xenobiotics, while a relatively fluid inner leaflet should facilitate insertion and diffusion of cytoplasmic peripheral proteins and hence accelerate surface reactions at the cytoplasmic leaflet. The high packing of the exoplasmic leaflet seems further to guide plasma membrane localization of single-pass transmembrane proteins with an asymmetrically shaped transmembrane domain[5], meaning that asymmetric packing could somehow guide protein transport. Interestingly, lipid order asymmetry is conserved in endosomes and lysosomes but probably absent in the endoplasmic reticulum or the Golgi apparatus[5], reinforcing the hypothesis that it might provide protection toward the outside media.

Q14 to membranes[43] and cell differentiation[10,44], as well as membrane fluidity at the immune synapse[15,45]. In a more recent application, spectral imaging was used to measure how muscle ageing is correlated with suboptimal fluidity of membranes in the muscle tissue[46]. In another study, the impact of modulating cellular glycosphingolipid metabolism and autophagy on myeloma bone disease via membrane fluidity remodeling was revealed[47]. Cell differentiation was also studied in the context of membrane fluidity. Matias et al. showed that alpha-ketoglutarate, a natural compound playing major role in cellular respiration, induces T cell differentiation via lipid remodeling, which results in changes in membrane fluidity[48]. Finally, as a new step in membrane fluidity measurements, high-throughput experiments have been performed in human serum-derived lipoproteins as well as viruses to show the membrane fluidity of thousands of particles in a single particle manner[49] (Box 2).

Comparison with other methods

Membrane fluidity can be measured by other means. As mentioned, ratiometric imaging of environment-sensitive probes gives insights about membrane fluidity via measuring membrane order. Similarly, diffusion of molecules residing in the membrane can be an estimate of membrane fluidity. Fluorescence correlation spectroscopy and fluorescence recovery after photobleaching have often been used to measure the diffusion in membranes[50]. Membrane

BOX 2

Fluidity of nanoscale bioparticles

Lipid bilayers are abundant in the human body beyond the cellular context. Small nanosized lipid particles and vesicles are used for molecular transport and cell–cell communication. Furthermore, pathogenic agents, bacteria and enveloped viruses possess their own lipid membranes, which are of great physiological importance for host cell infection. Lastly, a variety of drug delivery systems utilize nanoparticles containing lipid bilayers for targeted drug delivery as well as for protecting the active substance from immune responses.

Environment-sensitive probes have been employed for quantitative evaluation of the fluidity of such lipid bilayers. For example, fluidity of extracellular vesicles was studied in context of parasitical infections such as gastrointestinal parasites[92] and malaria[93]. For virus-like particles, the biophysical characterization of VLPs was performed for example for influenza[94], Ebola and Marburg viruses[95] as well as for HIV-1[96,97]. Yet, the majority of such measurements have been performed in cuvettes (or also by lipid extraction from virions and reforming them into artificial vesicles[97]), ignoring the possible heterogeneity of lipid order within the sample. Recent technologies enabled the analysis of single nanometer-sized particles in several fluorescence channels, which allowed for fluidity measurements in a high throughput manner[49]. This single particle profiling method was used to elucidate the fluidity of exosomes, virus-like particles, artificial liposomes and lipid nanoparticles. Such biophysical characterization of nanoscale bioparticles in health and disease can prove valuable for discovery of novel metabolic disease markers as well as novel drug targets.

fluidity via diffusion can also be inferred from single particle tracking measurements[51]. A less common technique to assess membrane fluidity via local viscosity of lipid membranes is fluorescence anisotropy[52,53]. Compared with these techniques, spectral imaging with environment-sensitive dyes is easier to implement. It can be performed with confocal microscopes and does not require a sophisticated data analysis pipeline. Throughput is also an advantage in spectral imaging since it is feasible to measure hundreds of cells in a short amount of time, while diffusion techniques are slow and limited to a few cells. On the other hand, the main advantage of the diffusion measurements with fluorescence correlation spectroscopy, fluorescence recovery after photobleaching and single particle tracking are that they are well-controlled experimental systems where absolute values can be determined and compared across different labs, while GP is an empirical parameter, which will be discussed in the 'Limitations' section.

Membrane fluidity can be determined by measuring changes in the photophysical properties of probes other than their spectra, such as fluorescence lifetime (Box 3). This approach is advantageous, since it does not rely on absolute intensity values, and, therefore, is not sensitive to variability introduced by improper staining or photobleaching. Among the lifetime-based techniques, fluorescence lifetime imaging microscopy (FLIM) measures viscosity of membranes by means of molecular rotors, which show a different relaxation time of fluorescence depending on the local viscosity[54]. However, lifetime decay curves need to be fitted with a proper model that requires prior assumptions on the number of lifetime components. The quality of the fit strongly depends on the total photon budget, especially when analyzing highly heterogeneous systems, such as live cells. Recently, it has been shown that the resolution in lifetime depends also on the range of wavelengths chosen to acquire the decay curves[55]. FLIM is also a relatively low-throughput, computational- and expertise-demanding technique[56].

BOX 3

FLIM to measure membrane fluidity

As an alternative to intensity-based spectral imaging of two-channel imaging, FLIM has several advantages. The fluorescence lifetime is an inherent property of a fluorophore, which is independent of absolute fluorescence intensity and fluorophore concentration. Further, fluorescence lifetime is not affected by nonuniform illumination and is less sensitive to absorption and scattering events compared with intensity-based measurements[56]. As excited fluorophores decay within nanoseconds, fast electronics together with efficient photon detectors are crucial for the temporal resolution required. FLIM can be implemented on wide-field illumination as well as laser scanning microscopy systems, and both frequency-domain and time-domain measurements are possible, the latter being the most common (time-correlated single photon counting)[56]. After acquisition of photon arrival histograms (fluorescence decays), the fluorescence lifetime is commonly estimated by curve fitting, deconvolution or phasor methods[56]. FLIM has a wide range of biological applications both in vitro and in vivo using autofluorescence[98,99] or fluorescent probes[100,101]. Further, FLIM–Förster resonance energy transfer measurements enable cellular interaction studies in vitro and in vivo[102–104].

One of the applications of FLIM is measuring membrane fluidity changes using fluorescent probes that change their fluorescent lifetime in response to their environment. Although often used in intensity-based imaging several solvatochromic probes, such as Laurdan[105], Di-4-ANEPPDHQ[106], push-pull pyrene dye PA[107] Nile Red[108], NR12S and NR12A[55], among others, also report on their environment by changes in their lifetime. Thereby, these probes have individual sensitivities to different lipid environments. As an alternative to solvatochromic dyes, mechanosensitive planarizable push–pull probes (commercialized as Flipper-TR) that incorporate into membranes have been developed and gained popularity[109,110]. Flipper has been shown to be sensitive to lipid packing as well as membrane tension[55]. Efforts to direct the Flipper probe location to specific organelles within the cell have been successful and allow an organelle-specific readout of lipid packing and membrane tension using FLIM[111]. Also molecular rotors such as BODIPY and derivatives can incorporate into membranes and report on membrane viscosity[112].

Application of these probes to measure fluidity of both synthetic and biological membranes is not trivial and requires strong expertise for reproducible data acquisition. In-depth characterization of the probes' lifetime in different lipid environments in crucial before application in more heterogeneous biological membranes[55]. Acquisition parameters such as laser repetition rate and detector settings need to be optimized for successful data analysis (for example, curve fitting) and lifetime resolution, respectively. Further, acquisition of sufficient photons for subsequent analysis needs to be ensured, resulting in long acquisition times (often slower than intensity-based imaging)[55,56].

Recent work has combined the use of environment-sensitive probes with flow cytometry to measure membrane fluidity in live cells in a high throughput and high correlative manner[29,57]. While flow cytometry allows a drastic increase in the number of measured cells, it requires robust probes and staining, as it does not provide the spatial resolution to assess probe localization and staining efficiency or uniformity. Imaging flow cytometry can provide low-resolution images, which can be sufficient to evaluate these parameters; however, the spectral flexibility to choose the optimal spectral regions can still be a limitation. This can be overcome with recent spectral flow cytometry tools[58]. There are other nonimaging techniques to measure membrane fluidity of model membranes such as nuclear magnetic resonance and surface plasmon resonance[59,60]; however, these techniques are low throughput and often not applicable to live cell measurements.

Limitations

GP is not an absolute parameter

GP values obtained from microscopy images highly depend on the optical setup as well as the wavelengths used for the calculations. Despite some efforts for interlab calibration using reference solvents and *G* factor[61], there is still a mismatch of GP values for model membranes of known lipid compositions. To account for differences caused by optical settings, instruments and external parameters that can vary daily, a known membrane can be measured before every measurement (such as 1,2-dioleoyl-sn-glycero-3-phosphocholine (DOPC)), and the data can be presented as the difference between the sample and the known membrane (ΔGP)[29]. Therefore, one should not take GP values in literature as absolute and should rather focus on differences in GP between samples for quantitative analysis.

Each probe is different

GP measurements are highly probe specific and monitor relative disorder within a particular system and using a particular microscope setup. For example, ΔGP between two experimental conditions could be different when different probes are employed. To be able to compare the absolute values across different experiments, the experimental setup and the probe should be the same. Therefore, the probes must be characterized rigorously in defined systems[55,62–65] for the following parameters in the next sections.

Probe behavior in the membrane

Our measurements are heavily influenced by the probe's ability to locate in the membrane and sense its environment. Therefore, our readout is very sensitive to any chemical and photophysical phenomena occurring in the probe's vicinity. For example, the sensing capabilities of probes depend heavily on their location in the membrane plane, for example, whether they are close to the head group of the lipids or buried deep in the acyl chain region[66,67]. Molecular dynamic simulations are often used to determine the probe location in the membrane plane, as performed for the localization of the probes we use in this protocol[63]. Additionally, the leaflet localization of the probes also affects the final readout. Most noninternalized probes are designed to reside in the outer leaflet of the plasma membrane, hence, they predominantly report therein[68,69]. Besides axial localization within the membrane plane, lateral partitioning of the probes in heterogeneous membranes should also be considered. For example, if a probe partitions predominantly into disordered domains, the final readout will be biased toward more fluid membranes. The ideal probe should exhibit equipartitioning. It is not trivial to account for this because measuring the partitioning of these probes in biologically relevant phase-separated membranes is challenging. Initially, such partitioning experiments of environment sensitive probes were performed in liposomes with either ordered or disordered membranes[70]; however it does not reflect the partitioning behavior when two phases coexist in a single membrane. Partitioning measurements for Laurdan in phase separated giant vesicles showed equipartitoning[70]; however, later it was shown that domains in giant vesicles are not representative of plasma membrane domains. This is a notable issue because depending on the packing of the membrane, both quantum yield and partitioning change[71,72]; hence, partitioning measurements need to be carried out in biologically

complex systems, such as giant plasma membrane vesicles (GPMVs)[73]. Even then, it is not easy to dissect whether the changes in fluorescence stem from partitioning or quantum yield differences in the two membrane environments. In summary, probe partitioning and quantum yield in domains stay as limitations for GP measurements, particularly when membrane heterogeneity is investigated. In this protocol, we do not aim to study membrane heterogeneity but rather overall membrane fluidity.

Probe localization in the cell

Ideally, the probes should localize in the structure of interest such as plasma membrane, mitochondrial membrane, lysosomal membrane and so on. Latest developments in dye localization have increased the efficiency of probe targeting into specific organelles[68,69,74] (Box 4). However, it is still technically challenging to achieve high targeting efficiency for different cell types. Although with different kinetics, all solvatochromic dyes will eventually internalize and diffuse into the intracellular environment; therefore, plasma membrane measurements might be limited to shorter acquisitions. Typical time ranges span from a few minutes to hours, depending on the selected dye and cell type.

Spatial and temporal resolution

Fluorescence microscopy is spatially limited by light diffraction, which restricts the maximum obtainable resolution to ~250 nm. Distinct lipid environments that are smaller or in closer proximity than the diffraction limit cannot be resolved. This limitation can be overcome by super-resolution imaging techniques. Nile Red-based plasma membrane polarity sensitive dyes are compatible with stimulated emission depletion (STED)[75,76] and single-molecule localization microscopy[69]. Super-resolution techniques, however, require more advanced equipment. In addition, our sensing ability of the environment is often limited by the temporal resolution of the instruments. The process of solvent relaxation (usually in a few nanoseconds) is significantly faster than image acquisition time, hence steady-state measurements of GP is the average

BOX 4

Organelle-specific environment-sensitive probes

While this protocol focuses on plasma membrane fluidity measurements, organelle fluidity can also be measured with the same protocol and by using organelle specific fluidity probes. Fluidity of intracellular membranes has been studied to a much lesser extent compared with the plasma membrane. Using unspecific probes to measure organelle fluidity is challenging as it requires robust image segmentation and colocalization with established organelle markers. This also implies that high throughput methods such as flow cytometry cannot be used for such purposes. Therefore, additional efforts have been made into expanding the environment-sensitive probe toolkit from plasma membrane specific probes to organelle specific probes.

The solvatochromic probes DXB-NIR and PK reveal polarity differences of lipid droplets and endoplasmic reticulum compared with the plasma membrane in live cells[113,114]. PK can also differentiate polarity in whole organisms (that is, zebra fish embryos) similar to Laurdan[28,114]. As the first probe to explore mitochondrial polarity by ratiometric imaging, BOB was used to examine differential mitochondrial polarity in cancer cells independent of membrane potential[115]. But also other probes such as NRTP[116], RCN[117] as well as RV-1 (ref. 118) and MMP[119] probe mitochondrial polarity, viscosity or both, respectively. Targeting specifically the lysosomes, Lyso-B is a BODIPY-based probe sensing lysosomal viscosity in live cells[120].

Recently, probes with the same solvatochromic unit but different organelle specificity have been developed to facilitate the comparison of fluidity of different organelles. One example is Nile Red derived probes, which were synthesized with chemical groups targeting ER, mitochondria, Golgi apparatus, lipid droplets and lysosomes, which can unravel organelle specific membrane fluidity[121]. For these probes, it is essential to evaluate the organelle targeting efficiency with well-established organelle specific markers.

Environment-sensitive probes can also be directed to specific organelles of nanoscale environments by genetic targeting. Haloalkane derivatives of BODIPY[122] or Flipper[123], which bind to Halo-tags, can be used to sense local microviscosity or membrane tension and lipid packing in live cells, respectively. Similarly, Nile Red has been conjugated to a Halo-tag binding group via a linker, to sense the polarity in the cytosol, endoplasmic reticulum, Golgi apparatus, inner and outer plasma membrane leaflet, as well as defined structures such as actin, microtubules and chromatin[124]. Nile Red has also been modified to bind the SNAP-tag to measure polarity, for example, around SNAP-tagged membrane proteins[125]. Further efforts have been made to customize Nile Red to specifically probe the lipid environment around GPCRs[126], the insulin receptor and GPI-anchored proteins[127].

of several relaxation events[77,78]. Therefore, the extent of the averaging depends on the dwell time and size of the focal spot, and these two parameters can be optimized for high-resolution fluidity measurements. For this purpose, time-resolved emission spectroscopy has been applied to observe the nanoscale development of solvent relaxation and other photophysical phenomena that environment sensitive probes undergo in membranes[62,77].

Experimental design

Overview of the protocol

The protocol (Fig. 2) starts with preparing the cells 1–2 d before the measurements (Steps 1–3). The microscope setup is calibrated with beads coated with a synthetic membrane of known fluidity (Steps 4–16). Next, the cells are labeled with environment-sensitive dyes (Steps 17–20). Imaging is performed using either two-channel or spectral imaging modality of the microscope (Steps 21–24), and the data are analyzed using a custom Fiji plugin (Steps 25–34).

Expertise needed to implement the protocol

Sample preparation requires familiarity with basic wet lab procedures and involves handling of small volumes (<1 mL) of chloroform. For cell sample preparation, cell culture experience is required. Albeit well established, confocal imaging might require user training; understanding the basic principles behind fluorescence microscopy is crucial for parameter optimization and high-quality data acquisition. Data analysis on ImageJ/Fiji benefits from knowledge on digital image fundamentals. The researchers with limited microscopy and image analysis skills should conduct initial experiments on robust controls. Lastly, researchers should observe national and local regulations regarding biosafety, cell culture, organic solvent handling and laser safety.

Experimental parameters

For robust measurements, it is crucial to have suitable probes and optical systems, prepare the samples properly and acquire and analyze the data carefully. In the next sections, we discuss these parameters.

Selecting a fluorescent probe. For optimal membrane fluidity measurements, solvatochromic probes should have certain properties. Ideally, they should be bright and fluorogenic, resulting in a high signal-to-noise ratio; strongly sensitive to immediate environment; suited for live-cell imaging at low concentration and toxicity; emissive in narrow emission bands to combine them with other probes; and specific to a certain cellular compartment (for example, plasma membrane with minimal internalization). The classical solvatochromic probes Prodan and

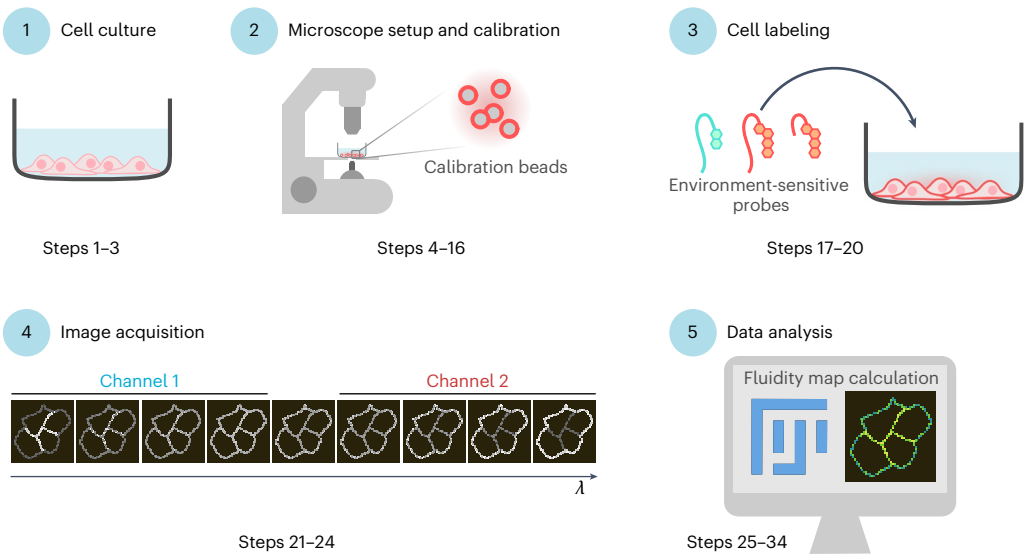

Fig. 2 | Overview of the protocol. The major parts of the protocol are shown with the associated procedure steps.

Laurdan were first used to study membranes in the early 1990s[25,79], and ~15 years later, di-4-ANEPPDHQ emerged[31]. While these probes have been widely used to study membrane fluidity in different contexts, they do not fulfil all the above-mentioned criteria[62,65]. High internalization rates and low photostability are the disadvantages of Laurdan[65]. Di-4-ANEPPDHQ[62], on the other hand, suffers from complex photophysics and a broad emission spectrum. While Nile Red exhibits solvatochromism, high photostability and fluorescence quantum yield, it is readily internalized and localizes to all membranes and, therefore, not suited for organelle-specific membrane fluidity measurements[80,81]. Probes used in this protocol are derived from the solvatochromic dyes Prodan/Laurdan (Pro12A)[68] and Nile Red (NR12A, NR12S and NR4A)[69]. These probes are plasma membrane specific and bright, covering different spectral regions. The protocol is also applicable to alternative solvatochromic dyes.

Of note, the biophysical mechanisms underlying the emission shift are not directly disclosed by the GP value or intensity ratios. Furthermore, it is often assumed that solvatochromic probes report on membrane properties in the same manner; however, in-depth characterization of Laurdan, di-4-ANEPPDHQ, NR12S, NR12A and Pro12A have revealed that probes exhibit different sensitivities to different liquid membrane properties[62,63]. This is mostly due to their diverse locations and orientations within the membrane[66]. Molecular dynamics simulations unraveled the locations of Laurdan and di-4-ANEPPDHQ[82], as well as Pro12A, NR12S and NR12A[63] in different lipid environments, which contributed to our understanding of probe response to their environment. For example, Pro12A is more sensitive to cholesterol content changes, while NR12A is able to sense lipid saturation with higher sensitivity[63]. Knowledge of these sensitivities is highly beneficial for application of these probes in different biological contexts. As such, it is advisable to combine data from probes, such as Pro12A and NR12S/NR12A, to obtain more information on the sample.

The spectral properties of the dyes are important factors to consider when selecting a dye (Table 1). NR12A is superior in terms of photostability and brightness, permitting the use of lower laser powers and dye concentrations. When using a second fluorescent tagged biomolecule, such as a fluorescent protein, the absorption/emission spectra of the fluorophores must be analyzed to avoid significant spectral overlap. In principle, NR12A and NR4A can be used in combination with blue-shifted fluorophores, while Pro12A allows the simultaneous use of red and far-red dyes. The absence of spectral overlap must be confirmed experimentally with sensitive spectroscopic or microscopic methods. An overlap can introduce a major bias in fluidity measurements where the sensor and fluorophore are in close proximity, since excited molecules can transfer energy through radiative or nonradiative processes, such as Förster resonance energy transfer, altering the measured emission spectrum and consequently the calculated GP values.

Concentration of the probes is also a crucial parameter, which should be low enough not to change the membrane properties itself but high enough to obtain a sufficient signal to noise ratio. At high concentrations, the probes themselves can change the fluidity[82], especially combined with continuous illumination. Table 1 suggests a concentration where we obtain enough signal to noise ratio, but the membranes are not affected by the probes.

Table 1 | Recommended dyes for plasma membrane fluidity quantification

Dye	Typical Excitation in confocal	Spectral bandwidth	Brightness	Channel 1	Channel 2	Labeling concentration	Photobleaching
Pro12A	405 nm	410–600 nm	+	440 nm	500 nm	200–500 nM	High
Laurdan	405 nm	410–600 nm	+	440 nm	500 nm	200–500 nM	High
NR12A	488, 561 nm	540–700 nm	+++	590 nm	650 nm	20–50 nM	Medium
NR12S	488, 561 nm	510–700 nm	++	570 nm	650 nm	200–500 nM	Medium
NR4A	488, 561 nm	540–700 nm	+++	590 nm	650 nm	200–500 nM	Low
Di-4-ANEPPDHQ	488 nm	500–700 nm	++	570 nm	650 nm	200–500 nM	Medium

Recommended concentrations are for spectral confocal imaging of cells. This may vary depending on the nature of the experiments and samples.

The time span of the experiment can also influence the choice of a fluorescent probe. When performing time-lapse measurements, one should opt for NR4A, as it allows for long-term imaging without photobleaching derived intensity loss due to its exchangeable nature[75]. The time between dye addition and measurement needs to be carefully considered to avoid biases derived from dye internalization ('Limitations' section). Ideally, dye internalization rates should be measured, as they can greatly differ among cell types.

Available systems and spectral versus two-channel imaging. Here, we will provide protocol for two different imaging modalities to measure membrane fluidity, namely two-channel and spectral imaging. Spectral imaging refers to the simultaneous acquisition of the whole emission spectrum of a fluorescent dye in every pixel of the microscopy image (Fig. 3a). This is typically achieved by using a diffraction grating, a prism or an acousto-optic modulator that spectrally disperses emitted light to an array of detectors, each of them constituting a spectral channel. During the last decade, microscope manufacturers have developed commercial setups equipped with spectral detection, often referred to as lambda imaging. It is, however, essential that all channels of the spectrum are obtained simultaneously with a single scan instead of a sequential scan of each channel. Sequential scanning will lead to inaccurate spectrum and fluidity values due to bleaching between the channel scans. Note that simultaneous spectral detection might not be included in default configurations and rather be offered as an optional module. Spectral imaging offers multiple advantages compared with the traditional two-channel approach. First, it provides higher fluidity resolution by selecting narrower spectral windows (Fig. 3b). This allows wavelength ranges showing the highest fluidity sensitivity to be chosen, thereby improving resolution as opposed to two-channel systems where typically broad emission windows are imaged. Additionally, spectral imaging provides information for advanced analyses, such as phasor plots, spectral unmixing or thresholding, which are not covered in this protocol. Naturally, by selecting a narrower detection window fewer photons are collected, decreasing signal-to-noise ratios and increasing statistical uncertainty (Fig. 3c). Therefore, for low labeling efficiency samples, one can either combine multiple spectral channels in different wavelength ranges or use two-channel imaging to increase signal at the expense of GP resolution (Fig. 3a).

Spectral imaging is not essential for fluidity measurements and might not be readily available to most researchers. Hence, it is important to note that this protocol is also applicable to microscopes not equipped with spectral detection. Spectral imaging is advantageous for the initial wavelength determination for the highest GP resolution (Fig. 3), but once these wavelengths are decided (which is provided in Table 1 for selected probes), any confocal

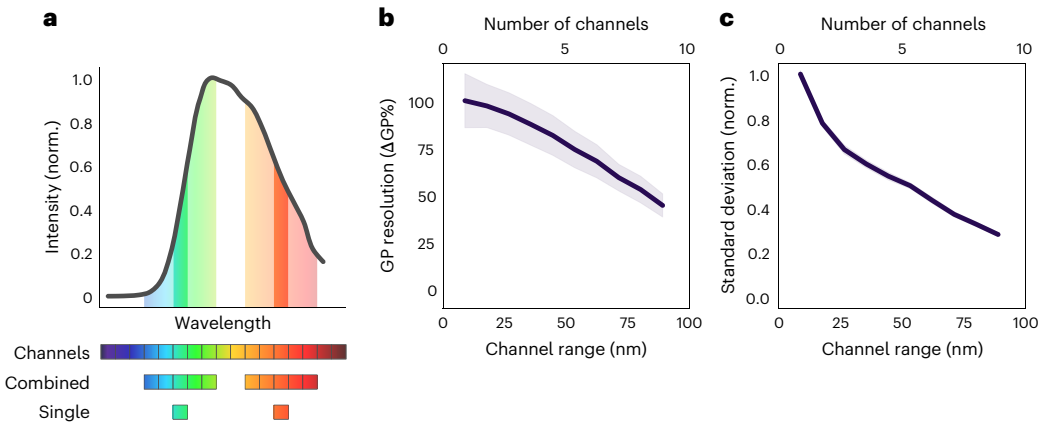

Q17 **Fig. 3 | Adjusting emission detection ranges for optimal GP resolution. a**, In spectral imaging, the emission signal is separated in multiple spectral channels. **b**, Combining channels decreases GP resolution, as measured by the difference in GP of NR12A between POPC and 1,2-diarachidoyl-sn-glycero-3-phosphocholine (DAPC) BSLBs upon combining of 9 nm spectral channels. The gray shaded area shows standard deviation of three experiments. **c**, The channel combination increases signal-to-noise ratios, resulting in higher GP precision. The conditions are the same as in **b**.

setup providing two spectrally separated channels in the suitable spectral range is applicable to perform fluidity measurements. Many commercial microscopes allow for manual tuning emission detection windows, while others rely on the use of fluorescent filters with fixed bandwidth. In the latter case, one should use filters that correspond to the lower and higher wavelengths of the emission spectrum (see Table 1 for ideal wavelengths for GP calculation). Note that in Table 1, as the breadth of collection range increases, GP resolution decreases (Fig. 3b); therefore, for two-channel imaging, one should choose a spectral range that is narrow enough for good GP resolution and broad enough for sufficient signal.

Sample preparation. Reliability and reproducibility of GP values require optimization of several parameters during sample preparation and data acquisition. First, before performing experiments in live cells, careful titration of the environment-sensitive dyes should be carried out. High concentrations of the probe might trigger internalization, diffusion into subcellular membranes or cell death. Thus, it is advisable to define an optimal dye concentration-per-cell number ratio and maintain it for the same set of experiments. The optimal ratio might change from dye to dye or in different cell types. Furthermore, the internalization rate of dye might be temperature- and time-dependent and could be minimized by operating at lower temperatures and with shorter incubations. Temperature is a critical parameter since, besides influencing the internalization rate of the probe, it can affect the fluidity of the lipid bilayer. Therefore, for the same set of experiments, it is important to perform the analysis of membrane fluidity under the same controlled temperature. Finally, for optimal image quality, high precision cover glass slides with 170 µm thickness should be used.

If cells need to be treated, for instance, with drugs or transfection agents, it needs to be performed before labeling the cells. Transfections are typically done 1–2 d before the experiment. The timing of drug treatments highly depends on the type of drugs and their mechanism of action. Membrane-modifying drugs, such as cyclodextrins, can show their effect within an hour. Metabolic drugs, which target certain pathways, can take up to days to show their effect. If a priori timing for the drug effect does not exist, a time-course experiment should be performed.

Data acquisition. To obtain reproducible GP measurements, it is crucial that the intensity values are well above background noise and lie within the dynamic range of the detector (that is, no saturation of pixels). Laser power and detector gain tuning is a straightforward way to ensure sufficient signal-to-noise and avoid saturation (Fig. 4). However, it is important to remember that these two parameters have a different effect on the total intensity; while the intensity increases linearly with increased laser power at low laser powers (linearity breaks at high laser powers as the fluorophores saturate), it increases in a nonlinear fashion with increased detector gain. Therefore, different combinations of laser power and gain levels should be tested to identify an optimal operation range.

Figure 4 shows the effect of laser power and detector gain levels on pixel intensity and GP distribution. Both the use of low laser power or detector gain result in low signal-to-noise ratios (Fig. 4b,d, top) with few pixels above the intensity threshold, leading to GP histograms with low pixel counts (Fig. 4a,c, top). On the other hand, too high laser power or detector gain cause pixel saturation (Fig. 4b,d, bottom), yielding GP values of 0 (Fig. 4a,c, bottom), since the pixel values in both channels are the same (equation (1)). These pixels are not informative and should be avoided by optimizing laser power and detector gain or removed during analysis. Appropriate laser power and detector gain will result in normally distributed GP histograms (Fig. 4a–d, middle).

After identifying the optimal laser power and detector gain combination, it is important to confirm the photostability of the probe under those conditions, as the excitation light can induce photobleaching, decreasing emission intensity (Fig. 5a). Moreover, bleaching might introduce artifacts in the measurement of membrane fluidity (Fig. 5b) and should be avoided by reducing laser power. According to equation (1), GP values should not be affected by a decrease in intensity due to photobleaching, since it is a ratiometric measurement. However, the plots in Fig. 5b suggest otherwise, particularly for NR12A, which shows an increase in

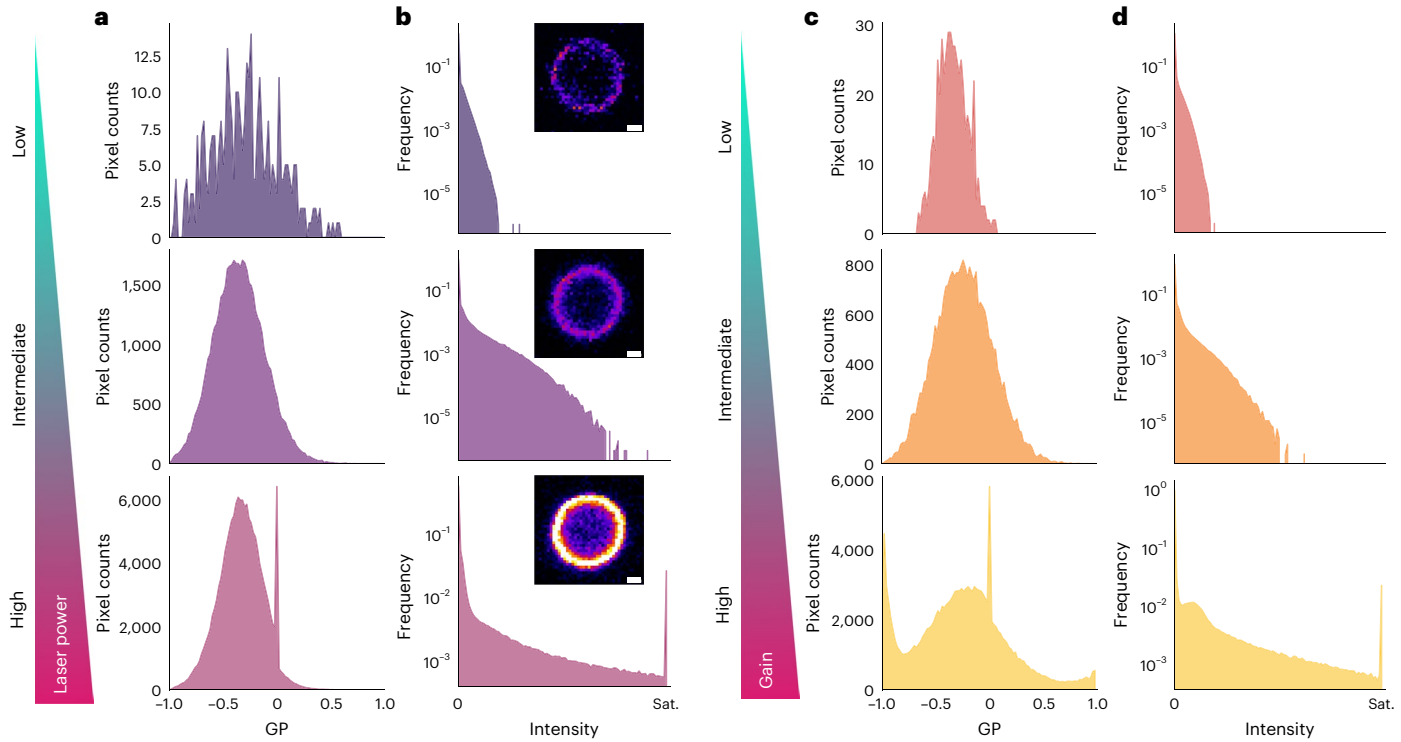

Q18

Fig. 4 | GP measurement as a function of pixels intensity. a,**b**, Effect of laser power on GP distribution and histograms of GP (**a**) and intensity values (**b**) at low (0.5%) (top), medium (3%) (middle) and high (18%) (bottom) laser power for channel 2 (λ = 646 nm) of spectral images of POPC-coated BSLBs stained with NR12A at constant detector gain (750 V). **c**,**d**, Effect of detector gain on GP distribution (scale bars, 1 µm) and histograms of GP (**c**) and intensity values (**d**) at low (650 V) (top), medium (750 V) (middle) and high (900 V) (bottom) detector gain for channel 2 (λ = 646 nm) of spectral images of POPC-coated BSLBs stained with NR12A at constant laser power (3%). Note that the recommended laser power and detector gain vary from system to system.

median GP with illumination time. This phenomenon might be ascribed to light-induced changes in the probe or the photoblueing effect, which would shift the emission toward shorter wavelengths, thus yielding apparent higher GP values[83]. For experiments requiring continuous sample illumination, we recommend using NR4A, since its exchangeable nature prevents photobleaching-induced signal loss and artifacts[75].

Another important factor to consider when analyzing membrane fluidity is the polarization of light. Some microscopes offer linearly polarized light, which will preferentially excite dyes in specific orientations due to photoselection[84], causing a difference in brightness along the directions perpendicular and parallel to the dipole moment of the laser beam. Large brightness differences can make thresholding challenging, requiring low threshold values and, subsequently, increasing the background contribution to the GP estimation. Due to this

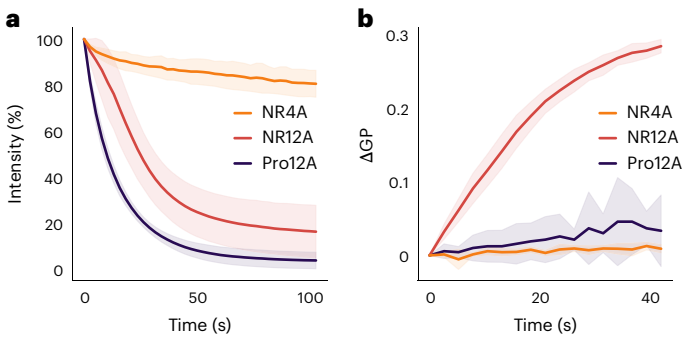

Fig. 5 | Effect of continuous illumination on intensity and GP. a, Continuous excitation of BSLBs labeled with Pro12A and NR12A induces photobleaching, causing signal loss. This is reduced by using the exchangeable probe NR4A. The mean image intensity normalized to the first value. **b**, Excitation light can also cause an artificial increase of GP. The lines are means, and the shaded areas are standard deviations of three independent measurements.

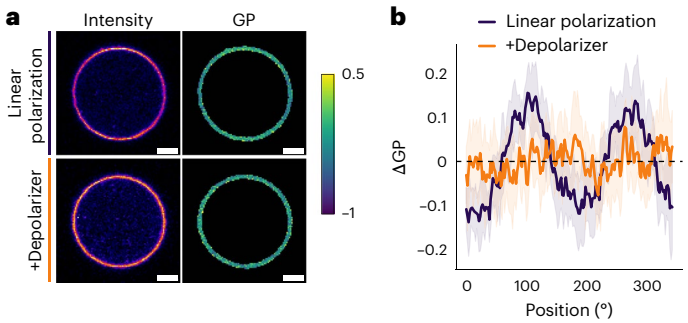

Fig. 6 | Polarization of the excitation beam can cause photoselection and artificial GP fluctuation in a single object. a, Intensity (left) and GP (right) images of NIH/3T3-derived GPMVs obtained by treating the cells with 25 mM PFA and 2 mM DTT in a buffer condition described previously[73]. Top: the vesicles stained with Pro12A show photoselection when excited with linearly polarized light, which is avoided by introducing a depolarizing element. Scale bars, 5 µm. **b**, Median GP values across the equatorial plane of Pro12A-stained GPMVs without (linear polarization) or with (+depolarizer) a depolarizing element. The lines are means, and the shaded areas are standard deviations of ten measurements.

preferential excitation, GP values will be lower in dimmer regions (i.e., perpendicular to the light polarization) and oscillate between a maximum and minimum value, when profiling along the membrane (Fig. 6a,b). By introducing a depolarizing element (often a quarter-wave plate) in the microscope's optical path, this effect will disappear, thus yielding a GP that varies only as a function of local environment (Fig. 6a,b). Finally, to avoid optical aberrations due to refractive index mismatch, it is advised to use water immersion objectives, since oil or air objectives can cause significant aberrations in live cell samples thicker than a few microns[85].

In conclusion, when setting up an experiment to measure membrane fluidity, one should follow the steps: (1) select a suitable dye compatible with the experiment (for example, good photostability for GP measurement over time, blue- or red-shifted emission for combination with other fluorescent dyes and so on); (2) identify optimal microscope settings (that is, laser power and detector gain) to avoid background noise and saturated pixels; (3) check for photostability of dye with selected microscope settings and, in case of photobleaching, retune laser power and detector gain accordingly; (4) utilize a depolarizing element to eliminate photoselection effects.

Calibration. Apart from optimizing the parameters mentioned above, system performance should be evaluated regularly (for example, monthly or bimonthly). ΔGP between two different lipid compositions, such as an ordered membrane (for example, 1,2-dipalmitoyl-sn-glycero-3-phosphocholine (DPPC):Chol) and a disordered membrane (DOPC or 1-palmitoyl-2-oleoyl-*sn*-glycero-3-phosphocholine (POPC)) is a robust way to perform this calibration (Fig. 8). During the first test with these calibration samples, wavelength ranges need to be determined to maximize GP resolution. In this protocol, we will calibrate the system with bead supported lipid bilayers (BSLBs) composed of DOPC, POPC and DPPC:Chol; however, it could also be performed using giant liposomes. BSLBs are robust membrane systems where lipid bilayers are formed on the surface of glass beads with well-defined size (we will use 5 µm in this protocol). They are easy to image, homogeneous in terms of size and lipid composition and their coating efficiency can readily be evaluated with the uniform and continuous membrane signal in microscopy images.

Data analysis. Accompanying this protocol, we include an ImageJ/Fiji macro tool implementing a user-friendly graphical interface to calculate GP values from spectral and two-channel data (Fig. 7). ImageJ and its refined version Fiji are powerful image processing programs that offer advanced functions for microscopy data analysis. Researchers with no coding experience can easily process images via the user interface, through the implemented functions or community-developed plugins. Given its widespread use, community resources and support are widely available online. Alternatively, users can employ other processing tools to analyze spectral imaging data, such as Python. We recently released an advanced software, VISION, based on Python with an easy-to-use graphical user interface[86], which allows to profile GP fluctuations along the membrane of individual cells and correlate these fluctuations with other biophysical properties or proteins expression. However, it is beyond the scope of this protocol.

The image analysis workflow starts by defining channel 1 (I_o) and channel 2 (I_d) for GP calculation (equation (1)). These can be two individual channels (number of channels of 1)

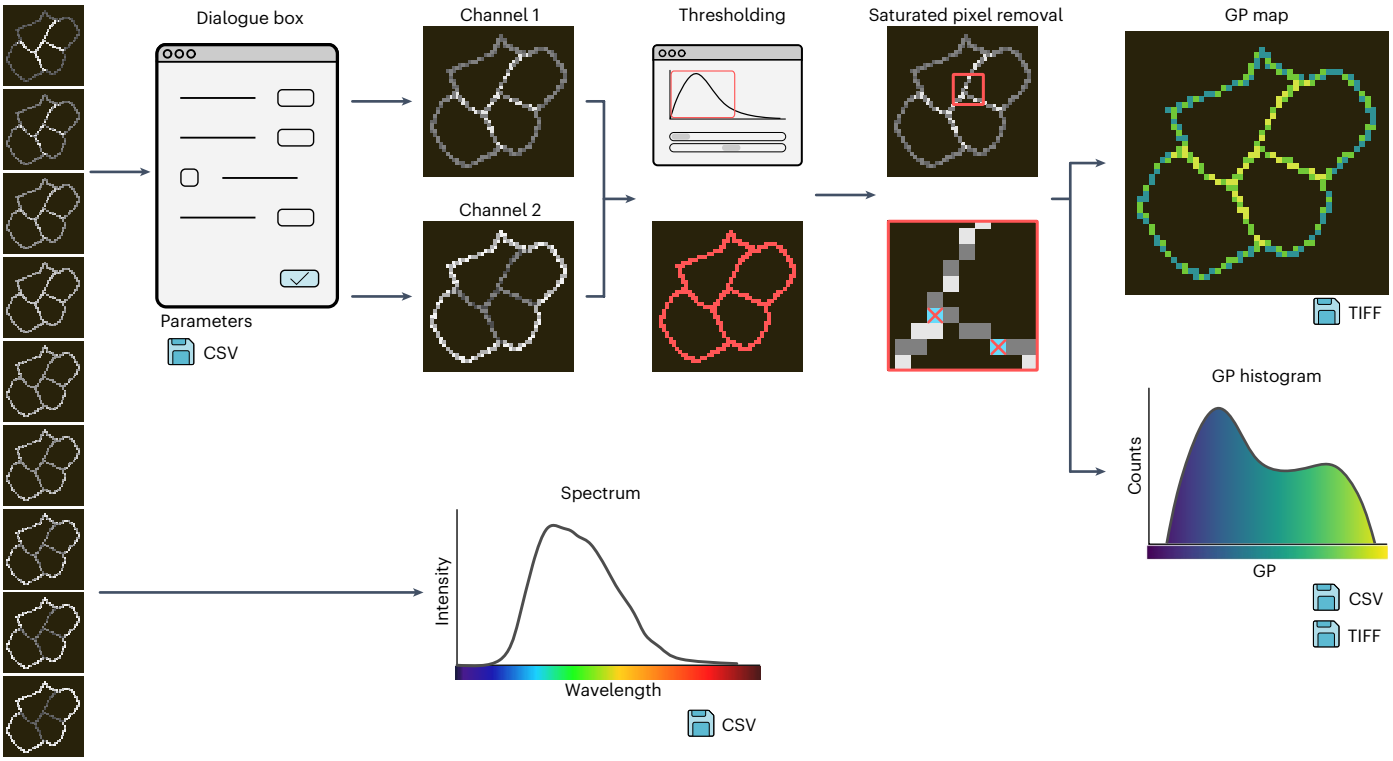

Fig. 7 | Image analysis pipeline. Details of image analysis are shown using the provided tool.

from spectral or two-channel acquisitions or a combination of consecutive spectral channels (number of channels >1) if increased signal-to-noise is required, at the expense of GP resolution (Fig. 3 and 'Available systems and spectral versus two-channel imaging' section). Then, thresholding is performed to select pixels within an intensity range to remove background signal. A mean filter can be applied to smoothen images during thresholding. Advanced options allow for thresholding in individual channels, although we recommend employing the sum of channels 1 and 2 as a reference for thresholding (the thresholding channel is defined as channel 1 + 2). Thresholding on individual channels can help in defining plasma membrane regions by filtering out internalized dyes by using channel 1, which would present a blue shifted signal. This can lead to bias of the obtained results and should be used only by advanced users. In the next step, saturated pixels are removed, as they do not represent the real emission signals and, thus, should not be used for GP quantification (Figs. 4 and 9). Only the pixels of channels belonging to channel 1 and channel 2 are evaluated for saturation. Lastly, the GP is calculated in all remaining pixels and presented to the user in a pseudocolored GP image, with some statistic parameters, such as GP histogram, median, mean and standard deviation. Critically, analysis parameters must be kept consistent to compare different experimental conditions.

Materials

Biological materials

- HeLa cells (ATTC, CCL-2, https://scicrunch.org/resolver/RRID:CVCL_0030)
- HEK-293T cells (ATTC, CRL-1573, https://scicrunch.org/resolver/RRID:CVCL_0045)
- NIH/3T3 cells (ATTC, CRL-1658, https://scicrunch.org/resolver/RRID:CVCL_0594)

▲ **CAUTION** The cell lines used in your research should be regularly checked to ensure they are authentic and are not infected with mycoplasma.

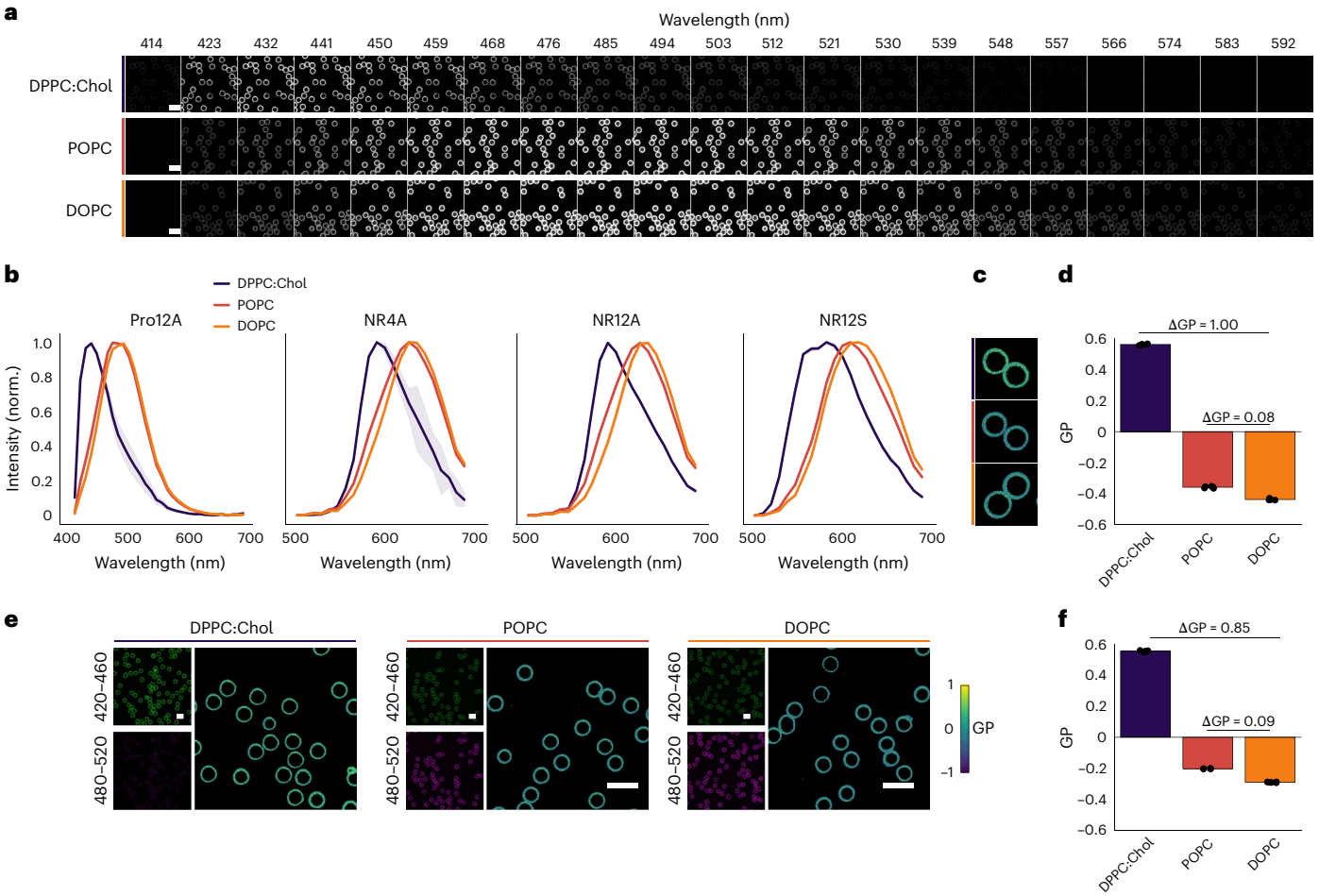

Fig. 8 | Calibration measurements of artificial membranes. a, Montage of Pro12A stained DPPC:Chol, POPC and DOPC BSLBs imaged with spectral module. **b**, Spectra of the probes in DPPC:Chol, POPC and DOPC BSLBs obtained from spectral images. The lines are means, and the shaded areas are standard deviations of three independent measurements. **c**,**d**, Representative GP images (**c**) and GP quantification (**d**) of Pro12A stained BSLBs. **e**,**f**, Two-channel confocal and GP images (**e**) and GP quantification (**f**) of DPPC:Chol, POPC and DOPC BSLBs stained with Pro12A. Scale bars, 10 µm.

Reagents

Dyes

- NR4A (Cytoskeleton, cat. no. MG06)
- NR12A (Cytoskeleton, cat. no. MG07)
- NR12S (Cytoskeleton, cat. no. MG08)
- Pro12A (Cytoskeleton, cat. no. MG09)
- DMSO (as dye solvent) (Merck, cat. no. D260)

Calibration

- POPC (Avanti Polar Lipids, cat. no. 850457)
- DOPC (Avanti Polar Lipids, cat. no. 850375)
- DPPC (Avanti Polar Lipids, cat. no. 850355)
- Cholesterol (Avanti Polar Lipids, cat. no. 700000)
- PBS tablets (Merck, cat. no. P4417)
- Liposome Buffer
  - 150 mM NaCl (Sigma-Aldrich, cat. no. S7653)
  - 10 mM HEPES (Sigma-Aldrich, cat. no. H4034)
  - Ultrapure water
  - NaOH (Sigma-Aldrich, cat. no. S5881)

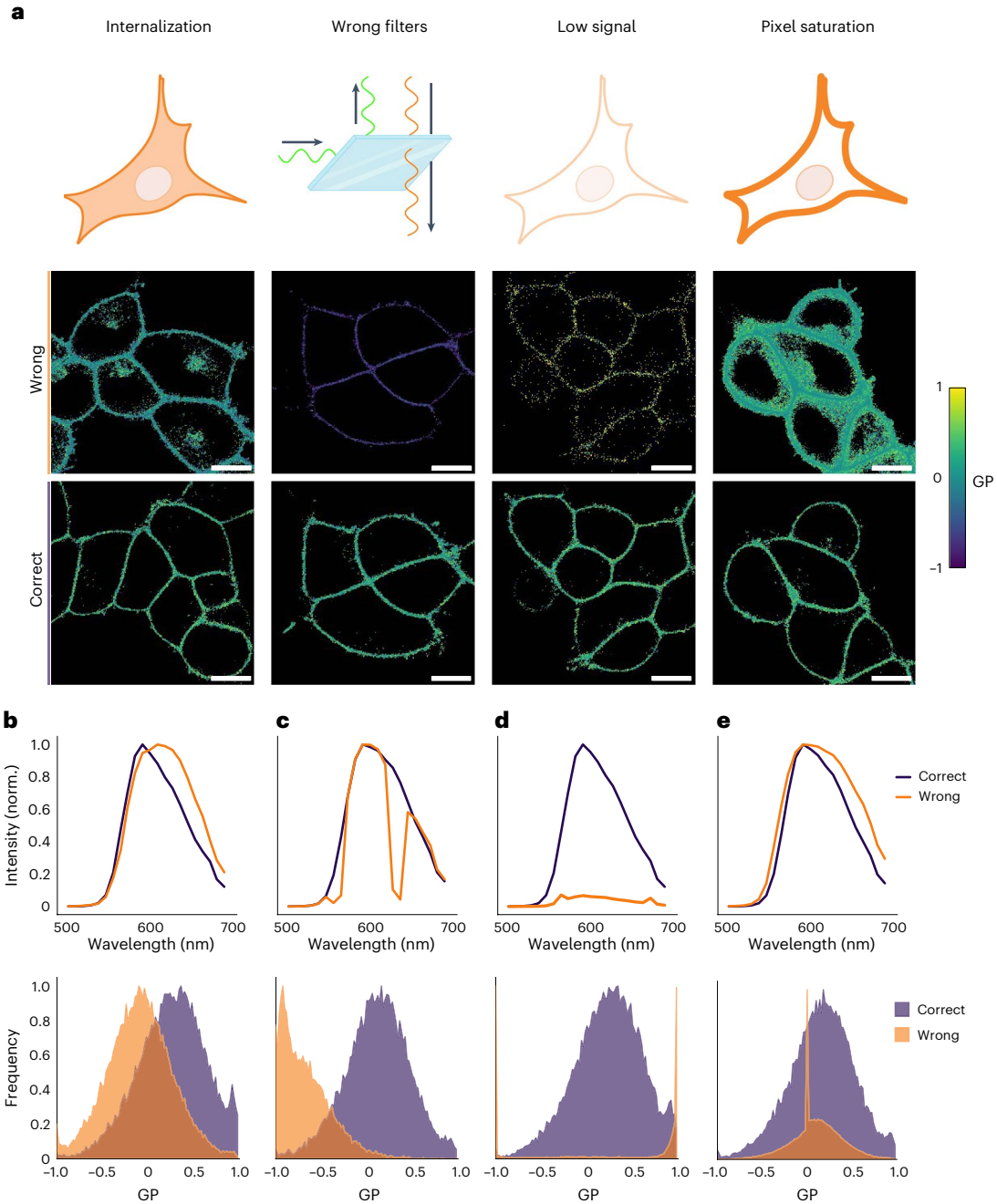

Fig. 9 | Common pitfalls and their impact on the emission spectra and GP histogram. a, Schematic presentation of common errors (first row) and their impact on the final GP map (second row) in HEK-293T cells labeled with 300 nM NR12A. For better comparison, the GP map using correct parameters is provided (third row) of the same field of view, whenever possible. Scale bars, 20 µm. **b**–**e**, The effects of each wrong parameter setting on the final normalized emission spectrum (top) and GP histogram (bottom) are shown.

- Chloroform (as lipid solvent) (Merck, cat. no. C2432)
  ▲ **CAUTION** Inhaling chloroform is hazardous due to its toxicity. Conduct steps involving chloroform in a fume hood.
- Silica beads, 5 µm (Bangs Laboratories, cat. no. SS05003)

Cell culture

- Dulbecco's modified Eagle medium (DMEM; Thermo Fisher Scientific, cat. no. 11965092)
- Fetal bovine serum (Merck, cat. no. F7524)
- Leibovitz's L-15 medium without phenol red (Thermo Fisher Scientific, cat. no. 21083027)

Equipment

- Laser scanning confocal microscope equipped with 40–60× water immersion objective lens ('Available systems and spectral versus two-channel imaging' in 'Introdiction'). The results presented here are obtained from Zeiss LSM 780 microscope with spectral GaAsP detector
- (Optional) Differential interference contrast slider (for example, Zeiss PA 63×/1.40 III, cat. no. 426957-0000-000)
  ▲ **CRITICAL** Circularly polarized light prevents photoselection in the *xy* plane, which changes measured GP values.
- Biosafety cabinet
- Incubator
- 1.5 mL tubes (Eppendorf, cat. no. 0030125150)
- Eight-well glass bottom microslides (Ibidi, cat. no. 80827)
- 25 cm^2 Culture flasks with vent cap (Corning, cat. no. 430639)
- Amber glass 2 mL vials (Merck, cat. no 27083-U)
- Screw cap for 2 mL vials with PTFE liner (Merck, cat. no 27091-U)
- Emmi 40HC Ultrasonic bath sonicator (Emag)
- Branson Ultrasonics Sonifier 250 (Branson)
- Microslide 18-well glass bottom (Ibidi, cat. no. 81817)
- Zetasizer Ultra Dynamic Light Scattering (Malvern)

Software

- Fiji, downloaded from https://fiji.sc
- Fluidity calculator from https://github.com/pcarravilla/fluiditycalculator/tree/main

Reagent setup

Cell growth medium

Prepare cell medium following the provider's instructions or guidelines from ATCC. Here, for HEK-293T, HeLa and NIH/3T3 cells we used DMEM (without pyruvate) complemented with 10% fetal bovine serum. Growth medium can be stored for up to 3 months at 4 °C. Always handle growth medium under sterile conditions.

Dye solutions

Dyes are usually provided as a lyophilized powder, which should be stored following manufacturer instructions. Before usage, resuspend the powder in DMSO and aliquot at 0.5–1 mM stock concentration. Prepare small volume aliquots to avoid repeated freeze–thaw cycles. DMSO-resuspended dyes should be kept at −20 °C and protected from the environment light. If preserved correctly, they can be stored for up to 2 years.

Liposome buffer

Mix the NaCl (final concentration of 150 mM) and HEPES buffer (final concentration of 10 mM) in ultrapure water. Then, adjust the pH to 7.4 with concentrated NaOH. This buffer can be stored at room temperature (21–25 °C) for up to a year if kept sterile.

Equipment setup

Install the analysis tool (first time only):

- An installation video guide for this can be found at https://www.youtube.com/watch?v=luqoejFVw4s
- Find your Fiji installation directory and navigate to the macros/toolsets folder
- Copy the file Fluidity Calculator.ijm file and the icons folder in the toolsets directory
- Copy the gp-viridis.lut file in the luts directory

Procedure

Cell seeding 1–2 d before the experiment

Q32 ● **TIMING 60 min**

1. Seed the cells on imaging slides. Seeding density varies among cell types, but a density of 50,000 cells/cm^2 can be used as a starting reference. Use glass or imaging-compatible polymer surfaces. Use no. 1.5 glass (0.17 mm thick, high precision) for best results. This protocol is optimized for adherent cells but can be adapted to suspension cells.
2. Grow cells for at least 24 h in growth medium until they reach 50–70% confluence. Depending on the cell type, alternative confluence levels might be desired. It is recommended that measurements are performed on cells showing matching confluency.
   ◆ **TROUBLESHOOTING**
3. (Optional) Expose the cells to the relevant treatment, for example, transfection or drug treatment ('Experimental design' section).
   ▲ **CRITICAL STEP** Avoid treating cells with toxic concentrations. Cell death will induce rapid internalization of fluorescent dyes that will then report on inner (and more fluid) cell membranes. Inner membrane labeling can be easily identified during imaging (Fig. 9).

Calibration sample preparation

● **TIMING 90 min**

▲ **CRITICAL** The following calibration steps (Step 4 and 5) should be followed only when evaluating the performance of the system, which should be carried out monthly or bimonthly.

4. Prepare liposomes as follows:
   - Transfer 10 µL from a stock of lipid solution (10 mg/mL in chloroform) into a 1.5 mL tube
     ▲ **CAUTION** Common laboratory pipettes are not optimized for retaining organic solvents and chloroform might leak during lipid solution handling. Use pipettes suited for organic solvents.
   - Dry up the lipid solution under a gentle nitrogen flow to evaporate all the chloroform from the lipid solution
   - Hydrate the lipid film with 1 mL liposome buffer and vortex vigorously to disperse all the lipid into the buffer. After vortexing, the lipid film should not be visible at the bottom of the tube, and the solution will appear turbulent. If the lipid film does not disappear from the bottom, incubate for a short time in a bath sonication (power 250 W, frequency 38 kHz) to promote dispersion
   - Wash the sonicator tip with ethanol and rinse it with water, insert the sonicator tip into the lipid dispersion, sonicate at output control 3 and pulse duration 0.4 s for 10 min. Once the sonication cycle has ended, the solution should appear clear. If the solution is still turbulent, try longer sonication times or use fresh lipid stocks or prepare fresh liposome buffer. Tip sonication might warm up the solution, thus affecting liposome formation. Keep the tube in an ice bath during the sonication to avoid temperature increase
   - Transfer the liposomes into a 1.5 mL tube
   - (Optional) Assess liposome size and homogeneity by dynamic light scattering. Too large liposomes or multiple populations with different sizes might affect coating efficiency
   - Flow nitrogen over the liposome solution to prevent oxidation, seal the tube with parafilm and store the liposomes at 4 °C until further use
     ■ **PAUSE POINT** Liposomes in a nitrogen atmosphere can be kept at 4 °C for 1–2 months.
     ◆ **TROUBLESHOOTING**
5. Prepare BSLBs from liposomes as follows:
   - Transfer 100 µL of liposome buffer into a 1.5 mL tube and add 1–5 µL of beads from a stock solution. Silica beads tend to sediment at the bottom of the tube; therefore, vortex the stock solution vigorously before handling

- Centrifuge for 2 min at 1,500*g*, discard the supernatant and resuspend the beads in the same volume of fresh buffer. Repeat three times. The storage solution for uncoated beads contains detergents. Thus, these washing steps increase coating efficiency and avoid liposome damage
- Vortex the liposome solution (from Step 4) vigorously, transfer 45 µL into the bead solution and add 355 µL of liposome buffer, to reach a final volume of 500 µL
- Incubate in a bath sonicator (power 250 W, frequency 38 kHz) for 30 min at room temperature. Alternatively, use a tube shaker at 2,000 rpm for 30 min at room temperature
- Centrifuge the coated beads at 1,500*g* for 2 min and remove the supernatant to remove excess liposomes. Resuspend the coated beads with 500 µL liposome buffer
  ■ **PAUSE POINT** Coated beads can be stored at 4 °C under nitrogen for 1–2 weeks.
  ◆ **TROUBLESHOOTING**
- Dilute the BSLBs in liposome buffer to a final volume of 100 µL
- Thaw the dye stock solution (in DMSO) and vortex it
- Add the dye to the BSLB solution to a final concentration (Table 1) and vortex vigorously. Nonuniform staining of BSLBs might be observed if the solution is not vortexed
- Transfer the stained BSLB solution into a microslide 18-well glass bottom chamber for imaging

Microscope set up

● **TIMING 10 min**

6. Switch on the microscope following manufacturer instructions.
7. Set the objective to a 40–60× water immersion objective lens. Oil immersion objectives result in different GP values at different axial planes due to the mismatch between the oil and medium refractive index.
8. (Optional) If the microscope does not provide circularly polarized light, insert the depolarizing element in the objective slot ('Data acquisition' section in 'Introduction' and Fig. 4).
9. Activate the required excitation lasers and let them stabilize for at least 30 min before imaging. Use 405 nm for Pro12A or 488 nm for NR12A/NR12S/NR4A. Set the laser power to 0.5–5 µW at the sample plane.
10. Set the appropriate beam splitter to separate excitation and emission light. The beam splitter should reflect excitation light toward the sample and allow transmission of the emitted photons to the detection path.
    ▲ **CRITICAL STEP** Ensure that the beam splitter does not filter out part of the emitted signal. Some manufacturers include beam splitters that are compatible with multiple excitation wavelengths (for example, 488/561/640 nm) and can overlap with the emission spectrum, inducing artifacts in GP calculations, as part of the emission signal would be filtered out by the beam splitter (Fig. 9).
11. Set up the microscope for spectral (option A) or two-channel (option B) detection ('Available systems and spectral versus two-channel imaging' section in 'Introduction').
    ▲ **CRITICAL STEP** Researchers might want to employ a reference fluorescent signal, for example, a protein of interest tagged with a fluorescent protein to identify transfected cells or to mask pixels of interest. This can introduce biases in GP calculations ('Selecting a fluorescent probe' section in 'Introduciton'). Before proceeding, the lack of spectral overlap should be confirmed by highly sensitive spectroscopic methods and adequate controls. In that case, make sure that each dye is excited, and its emission is collected sequentially.
    (A) **Spectral imaging**
    (i) Activate the spectral detection mode, sometimes referred to as lambda mode.
    (ii) Set the width of each channel to ~9 nm, which offers adequate signal-to-noise ratios and allows simultaneous detection of the full spectrum.
    (iii) Set the spectral range to span all the emission spectrum of the dye. Use 410–600 nm for Pro12A or 500–690 nm for NR12A/NR4A.

(B) **Two-channel imaging**

(i) Activate two detection channels within the same imaging track, so that signals in both channels are acquired simultaneously upon excitation.

(ii) Set the emission window for each detector to channel 1 and channel 2 ranges. For Pro12A use 420–460 nm (centered ~440 nm) and 480–520 nm (centered ~500 nm). For NR12A/NR4A use 570-610 nm (centered ~590 nm) and 630–670 nm (centered ~650 nm). For NR12S, use 550–590 nm (centered ~570 nm) and 630–670 nm (centered ~650 nm). If the microscope does not allow for manually tuning emission detection windows and instead emission filters are used, choose filters that resolve GP changes. For example, when using NR12A, typical orange (580–630 nm, for example, Cy3 filter) and red (650–700 nm, for example, Cy5 filter) filters can be employed.

12. Adjust detector gain. The voltage values ~650–800 V usually provide adequate signal-to-noise ratios. Note that these values can vary depending on the system or the type of detector being used.
◆ **TROUBLESHOOTING**
13. Set the pinhole to 1 airy unit.
14. Select the overall image size according to your sample. Set the pixel size to 80–100 nm, following the Nyquist sampling criterion. Some systems allow for automatic optimal size selection. Make sure that a constant pixel size is being used. In some systems, the pixel size has to be updated every time the size of the sampling area (zoom level) is modified. Pixel size is a critical parameter to ensure maximal spatial resolution. In some microscopes pixel size is adjusted by changing the number of pixels of the image.
15. Adjust the pixel dwell time to 0.5–2 µs. It can be set to longer times to increase emission signal; however, long dwell times might result in increased photobleaching rates.
16. Set line averaging or accumulation to 1–4 depending on the noise in the images; use higher averaging in noisy images.

Cell labeling

● **TIMING 15 min**

▲ **CRITICAL** These steps are for the actual cellular measurements; therefore, they are not needed for calibration. For calibration only, please proceed to Step 21.

17. Wash the cells 2× with serum-free imaging medium. Choose L-15 medium if the microscope is not equipped with a CO_2 incubator, as it is buffered by phosphates and free base amino acids that do not require high CO_2 concentrations as conventional buffers, such as DMEM.
▲ **CRITICAL STEP** Labeling in serum-supplemented media is suboptimal as the dye is taken up predominantly by the lipid particles in serum. Hence, it is important that serum is completely washed away, and the labeling medium does not contain serum.
18. Prepare the labeling solution in a tube by dissolving the DMSO-dissolved dye in the serum-free imaging medium and homogenize by vortexing for 5 s.
▲ **CRITICAL STEP** Dye concentration needs to be optimized depending on cell type, cell density or labeling medium. As a starting reference, use 100–200 nM Pro12A, 20–50 nM NR12A, 200–500 nM NR12S and 200–500 nM NR4A. Minimize added DMSO volume by adjusting stock concentrations, as high concentrations of DMSO can be toxic to cells, resulting in cell death and dye internalization.
19. Replace the medium from the previous washing step with the labeling solution and incubate in the dyes for 2 min. Timing can vary depending on the cell type. Leave one well unstained to assess autofluorescence.
▲ **CRITICAL STEP** In some cell types, dyes might show rapid internalization rates, which results in biased GP values, as internal membranes constitute high fluidity environments ('Limitations' section). In that case, consider using an alternative dye. If this is not possible, add dyes immediately before imaging and make sure imaging sessions do not exceed internalization times.

20. (Optional) Wash the cells 1× with imaging medium. These probes are fluorogenic, that is, they are fluorescent only when in the membrane. Therefore, unbound molecules do not result in significant background signal. Do not wash when using NR4A, due to its exchangeable nature, most of NR4A is expected to stay in solution.
◆ **TROUBLESHOOTING**

Image acquisition

● **TIMING 1 h**

21. Apply the appropriate immersion medium and place the slide/chamber on the microscope objective lens (Steps 6–16).
22. Focus on the fluorescently labeled cells (or BSLBs if calibrating the system) and fine focus on the equatorial plane. The bottom and top regions might suffer from photoselection effects. Avoid imaging dead/dying cells, which can be identified due to high dye internalization.
◆ **TROUBLESHOOTING**
23. Acquire an image. If image quality is not adequate, for example, low signal-to-noise ratio or saturated pixel, adjust imaging settings (Steps 12–16). Avoid using high laser powers that can induce phototoxic reactions.
▲ **CRITICAL STEP** Imaging settings should be kept consistent throughout the experiment. Do not compare GP values acquired using different microscope parameters or in different instruments.
▲ **CRITICAL STEP** At this step, it is critical to image an unstained sample to rule out the contribution of any autofluorescence.
◆ **TROUBLESHOOTING**
24. Save images in an appropriate format. Fiji can open most proprietary microscopy formats through the Bio-Formats Importer.

Data analysis

● **TIMING 1 h**

25. Click in 'More Tools' menu in the 'Toolbar' (right most double arrow) and select 'Fluidity Calculator' (this step has to be performed every time Fiji is launched).
26. Open/import an image. The analysis program requires fluorescent channels to belong to a single image.
    - If channels are imported as individual images, adjust import options, for example, uncheck the 'Split channels' option in the 'Bio-Formats Import Options' window, which can be accessed through 'Plugins → Bio-Formats → Bio-Formats Importer'.
    - Alternatively, combine different channels in a single image using: 'Image → Color→Merge Channels'.

    The analysis macro tool also requires that channels and time frames are labeled as such. Sometimes incorrect import options can mislabel channels as *z* slices or frames. Adjust import options or reassign stack labels: Image → Hyperstack → Reorder Hyperstack.
27. (Optional) Select a region of interest and use the 'Duplicate' function to generate a new image containing only the region of interest.
28. Select the image to be analyzed and click on the fluidity calculator icon on the 'Toolbar'.
29. Set the analysis parameters. A list of parameters is given in Box 5. Settings should be kept consistent throughout the analysis. Do not compare images analyzed using different analysis parameters. The documentation for these parameters can be accessed by pressing the 'Help' button.
30. Set an intensity threshold. Only pixels within the thresholded region will be used for GP analysis. Ensure that the threshold is significantly above the background signal ('Data acquisition' section in 'Introduction' Fig. 4).
31. Press OK to display the GP image, along with a histogram and a table with statistical parameters. Only pixels above the user-defined threshold and not saturated are considered for quantification of statistical values (mean, median and standard deviation) and the histogram. If a single fluidity environment is expected, the histogram should display a normal distribution of GP values.

BOX 5

Parameters for the fluidity calculator

(i) Channel 1 and channel 2 are assigned to I_o and I_d, respectively, in equation (1).
(ii) For Pro12A use 440/500 nm, for NR12A/NR4A use 590/650 nm. If such values are not listed, use the closest possible value, for example, 441/503 nm instead of 440/500 nm.
(iii) Channel window range is the number of spectral channels that will be combined for channel 1 and channel 2 (Fig. 4). Users can choose any set of wavelengths as long as they do not overlap, that is, while they are not used for both channels.
(iv) The channel selected in the channel 1/channel 2 list will be in the middle of the range, that is, when selecting the 590 nm channel as (1) channel 2 and (2) channel window range of 3, the channels corresponding to 581 nm, 590 nm and 599 nm will be combined and assigned to channel 1.
(v) Checking the 'Mean Filter' checkbox will apply a mean filter to the thresholding image. Note that GP calculations will still be performed on raw intensity values, that is, ignoring the filter. If signal-to-noise is high enough, we recommend not using this option.
(vi) The mean filter radius is the number of pixels used to calculate the 'Mean Filter' for thresholding.
(vii) Thresholding channel is the channel that will be used for thresholding. The default channel 1 + 2 should be used. Selecting the channel 1 or channel 2 options can result in overestimation or underestimation of GP values, respectively. For example, thresholding pixels according to their signal in channel 1 will result in preferential selection of pixels displaying higher GP values, causing an artificial increase. Only use this option for advance thresholding, for example, to threshold the plasma membrane of cells displaying high amounts of internalized dyes. However, it is recommended to avoid such cases by optimizing the imaging parameters (laser power and gain).
(viii) The saturated pixel warning percent value will result in a warning when the number of saturated pixels within the thresholded region is above this percentage.
(ix) Note that these pixels will be removed from the analysis, regardless of the saturated pixel warning percent value.
(x) Activate the 'Calculate Emission Spectrum' checkbox to show the emission spectrum average of all pixels within the threshold. This feature only works for images with more than five channels.
(xi) Activate the 'Save Results' checkbox to save the analyzed TIFF image and CSV files containing the used parameters, calculated statistics and the GP histogram.
(xii) The 'Save Analysis Mask' checkbox will save a mask tiff image showing the pixels that were considered for GP analysis. These are the pixels within the threshold set by the user as long as they are not saturated.
(xiii) The 'Save To' option is used to select the directory where the images and CSV files will be saved.
(xiv) Activate the 'Save as Default Settings' checkbox to save the used settings as default.

▲ **CRITICAL STEP** A 'Saturated Pixel Warning!' window will appear if the number of saturated pixels within the area selected through thresholding exceeds the 'Saturated Pixel Warning %' value set in Box 5 (vi). If the saturated pixels are from the structure of interest and exceed the limit, we recommend not to continue as the remaining pixels will not be representative of the whole image. If the percent value is below the limit, press OK to continue.

32. (Optional) Change the look-up table (LUT) of the GP image from the Fiji 'LUT Menu'. We recommend viridis, which is a color-blind friendly LUT. Other LUTs available in Fiji such as magma, plasma, inferno or turbo are also suitable for GP visualization.
33. Define regions of interest around individual cells or specific areas using the Fiji image selection tools, such as 'Polygon selections' or 'Freehand selections' in the 'Toolbar'. Press the 'Live' option in the 'Histogram' window to display an updated histogram of the selected area. Use 'Analyze → Measure' to record the parameters of that region. Calculated parameters are defined in 'Analyze → Set Measurements'.
34. For quantitative comparison, store the median GP value if a single population is observed in the histogram. Three independent biological replicates should be performed for each condition to ensure data robustness and significance.

Troubleshooting

Troubleshooting advice can be found in Table 2.

Table 2 | Troubleshooting table

Step	Problem	Possible Reason	Solution
2	Cells do not or only loosely attach to the imaging slide	Surface properties not optimal for cells	Coat the glass surface with poly-D/L-lysine, gelatin or laminin
4	Impurities and aggregates are visible in the liposome solution after sonication	Contamination from the sonicator tip, for example, old tip	Pellet down impurities by centrifugation (10,000*g*, 3 min) and transfer clean supernatant into fresh tube
			Replace sonicator tip
5	Beads are not fully coated	BSLBs, lipid stocks or buffer have been stored for too long	Try fresh lipid stock and fresh liposome buffer. Prepare BSLBs fresh
12	High noise contribution in the images	Detector gain too high	Increase dye concentration, laser power, pixel dwell time or line averaging and decrease the gain
20	Fluorescence signal very dim or equal to autofluorescence control without dye	Dye-to-cell ratio too low	Use higher dye concentration to increase the dye-to-cell ratio
		Labeling time too short	Increase labeling times and omit the washing step
		High cell autofluorescence	Use a cell line with low autofluorescence or a dye whose emission does not overlap with the autofluorescence
		Wrong microscope parameters (excitation, emission)	Thoroughly check laser and filter settings are correct
	Strong intracellular fluorescence	Labeling temperature too high	Decrease labeling temperature to room temperature
		Labeling time too long	Try shorter labeling times
		Local or global concentration of solvent (DMSO) too high	Prepare higher concentrated stock solution of dye to dilute solute during labeling
22	High number of dead cells	Toxic dye/solute concentrations	Decrease the dye/solute concentrations
		Suboptimal live-cell conditions	Minimize shear forces and time outside the incubator
			Include AnnexinV-647 labeling to detect apoptotic cells and exclude them from the analysis
23	Image shows high amount of low intensity or saturated pixels	Suboptimal microscope settings	Adjust the gain, laser excitation, pixel dwell time, line averaging and pixel size to decrease the amount of low intensity and saturated pixels. Intensity values of regions of interest should be centered in the intensity histogram

Timing

Steps 1–3, cell seeding: 1–2 d before the experiment: 60 min
Steps 4–5, calibration sample preparation: 90 min
Steps 6–16, microscope set up: 10 min
Steps 17–20, cell labeling: 15 min
Steps 21–24, image acquisition: 60 min
Steps 25–34, data analysis: 60 min

Anticipated results

This protocol can be used for model membranes (such as giant vesicles, cell-derived vesicles and liposomes) and in live cells. Here, we show how our protocol can enable robust and fast measurement of changes in membrane fluidity of mammalian cells. Before the cellular measurements, an initial calibration measurement with known lipid membranes is performed to determine and maximize the system performance. As detailed in the Protocol, DOPC,

POPC and DPPC:Chol membranes can be used for this purpose. Figure 8a shows montages of spectral images of DOPC, POPC and DPPC:Chol BSLBs stained with Pro12A. Emission spectra of the environment sensitive probes Pro12A, NR12A, NR12S and NR4A in these membranes obtained from spectral imaging are shown in Fig. 8b. As observed from the spectra, the difference between DOPC and POPC is small; therefore, the probes and wavelengths should be selected properly to be able to resolve this difference. DPPC:Chol is significantly more ordered compared with other two as indicated by the peak in fluorescence intensities in the lower wavelengths; therefore, GP difference between DPPC:Chol and DOPC is a good estimate of the dynamic range of the system. Figure 8c,d shows the GP images of BSLBs made of these three membranes and the GP values obtained from them when we use Pro12A in combination with spectral imaging and single channels for GP calculations as indicated in Table 1. ΔGP between DOPC and POPC is ~0.08 GP unit while between DOPC and DPPC:Chol is ~1.0 GP unit. When two-channel imaging is used with the wavelength intervals specified in Table 1, ΔGP between DOPC and POPC is similar to that obtained with spectral imaging; however, ΔGP between DOPC and DPPC:Chol is smaller compared with spectral imaging (Fig. 8e,f) as previously discussed (Fig. 3).

For cellular measurements, one can encounter pitfalls, which might cause unreliable GP measurements in cells and should be avoided (Fig. 9). Here, we describe the results when each step is performed properly. Moreover, we show common pitfalls and their impact on GP values as well as how they can be identified from emission spectra or GP histograms.

Several parameters can lead to increased internalization rates of environment-sensitive dyes and impede reliable plasma membrane GP measurements due to the signal from intracellular membranes. In our experience, the parameters influencing dye internalization rates most heavily are labeling time, dye characteristics, temperature, dye concentration, cell line, plasma membrane integrity and local concentration of the solvent (for example, DMSO). Longer labeling times lead to increased internalization of the environment-sensitive dyes, which is accompanied by a decrease of GP values (Fig. 9a,b). Typically, the inner leaflet of the plasma membrane, as well as intracellular membranes, are more fluid and will, therefore, shift the median GP value to smaller values. For this reason, it is important to perform the labeling and acquisition within a consistent time window. Increased internalization can be clearly identified from intracellular dye signal and a total decrease of GP values without additional treatment. From our experience, the total time for labeling and acquisition should not exceed 20 min when imaging at room temperature but needs to be determined for each cell line and dye combination. Conventional probes, such as Laurdan, shows fast internalization rates that are drastically reduced in the case of Pro12A, NR12A and NR4A. We recommend evaluating the rate of internalization at different concentrations for each cell line before the actual experiment.

Wrong filter settings can block out spectral regions essential for GP calculation and lead to incomplete recordings of emission spectra of the environment-sensitive dyes (Fig. 9a,c). Typically, dichroic mirrors and emission filters intended to reflect and block out excitation lasers, respectively, are the cause of these incomplete spectra. This mistake can be easily identified by checking the full emission spectra for missing parts. If any of the channels used for GP calculation overlap with such blocked emission windows, the resulting GP values will be incorrect (Fig. 9c). If none of the available filter sets let the full spectrum through, it is crucial to use channels that are clearly outside of the filtered-out emission range.

In fluorescence microscopy, recording saturated and low signal pixels should generally be avoided. It is advisable to record the fluorescence signal within the dynamic range of possible gray values, clear of minimal (0) or maximal (saturated) values. If the recorded fluorescence signal is very dim, the contribution of noise will increase and cause artificial GP values close to −1 and +1 (Fig. 9a,d). Therefore, we recommend checking the final GP histogram to ensure that the main populations are not converging to −1 or +1. If the laser power or gain is set too high, the number of saturated pixels—that is, pixels reaching the maximum possible gray value—will increase and their real intensity value is lost (Fig. 4). If the signal of both channels is saturated, an inaccurate GP of 0 pixel population will appear (Figs. 9a,e and 10).

Occasionally, it is inevitable that there will be a small number of saturated pixels in the image even with optimal imaging settings, such as at cell-to-cell contact areas where the dye

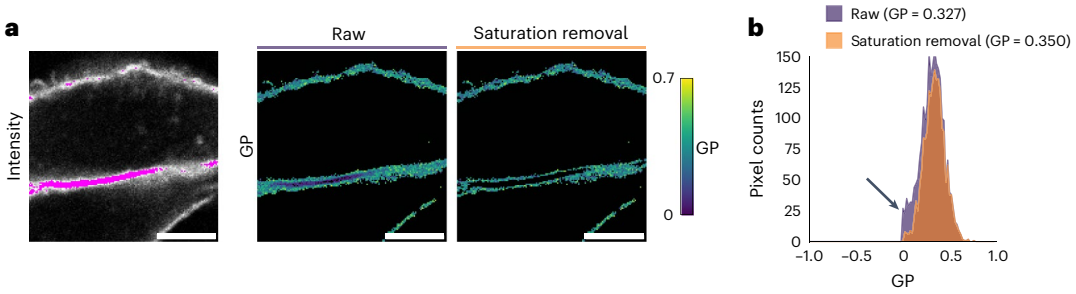

Fig. 10 | Saturated pixel correction. a, Saturated pixels (magenta in the intensity image) lead to GP = 0 values, which should be excluded from GP images. Scale bar, 5 µm. **b**, The GP histograms of the image in **a**. The saturated pixels can be identified in the histogram as a GP = 0 population (arrow). If not excluded, saturation will artificially shift the GP distribution.

concentration is doubled or in intracellular structures with high intensity. This will lead to the characteristic artificial GP of 0 population, shifting median GP values toward 0 (Fig. 9). Our provided ImageJ/Fiji macro tool automatically excludes saturated pixels from further GP calculation and enables the user to analyze only unsaturated pixels, yielding correct GP values (Fig. 10). However, this should only be done when only a small number of pixels are saturated, or the saturated pixels are from structures that are not of interest. If a large number of pixels from the structure of interest are saturated, those images should be discarded, as the saturation correction will bias the GP results by omitting the saturated pixels.

Additionally, it is strongly encouraged to acquire autofluorescence controls of unlabeled cells using the final microscope settings to exclude autofluorescence artifacts. Biological samples can show a high degree of autofluorescence, and it is necessary to use a threshold during analysis that is well above this autofluorescent signal by ensuring high signal-to-noise ratios and optimal labeling conditions.

Before starting with the cellular fluidity measurements, we highly recommend validating the compatibility and dynamic range of the used setup and experimental conditions. This can be performed by a cholesterol removal experiment typically leading to a significant increase of fluidity, which can be quantified by a decrease of the GP value[26] as well as increase in diffusion[87]. A fast and easy way for cholesterol removal is the treatment with the water-soluble oligosaccharide methyl-β-cyclodextrin (MβCD). The optimal MβCD concentration and incubation time is highly dependent on the cell line used and should be determined beforehand or obtained from literature to guarantee sufficient cholesterol removal while maintaining cellular viability[88–90]. For initial experiments, we recommend using a concentration between 1 and 10 mM and 30 min incubation. Using optimal conditions, MβCD treatment will cause a robust and reproducible GP value reduction (Fig. 11a,b). In the following part, we highlight how the pitfalls described can perturb the reliable detection of fluidity changes due to cholesterol removal. The global decrease of GP by increased dye internalization impedes the robust detection of cholesterol removal by MβCD treatment (Fig. 11a,c). Moreover, too-high laser power or gain can cause an increased amount of saturated pixels, leading to an artificial increase of GP values equal to 0 and impede the detection of MβCD-induced increase in fluidity (Fig. 11a,d). Finally, the use of inadequate filter settings that block out valuable emission information can lead to a global shift of the GP distribution toward −1 or +1 (Fig. 11a,e) and do not allow for the detection of cholesterol removal. Altogether, these examples highlight the importance of correct and consistent protocol parameters for the reliable detection of biophysical changes of cellular membranes using environment-sensitive dyes and spectral imaging.

Finally, we present an example of time lapse imaging of cells. For this purpose, we stained HeLa cells with NR4A and imaged for 30 min by taking an image for every 30 s. We encourage to use NR4A for time-lapse imaging because it is an exchangeable probe and, hence, does not show strong internalization or bleaching[75]. Figure 12a shows representative images of NR4A-labeled cells, either untreated or treated with calcium ionophore A23187, which scrambles the plasma

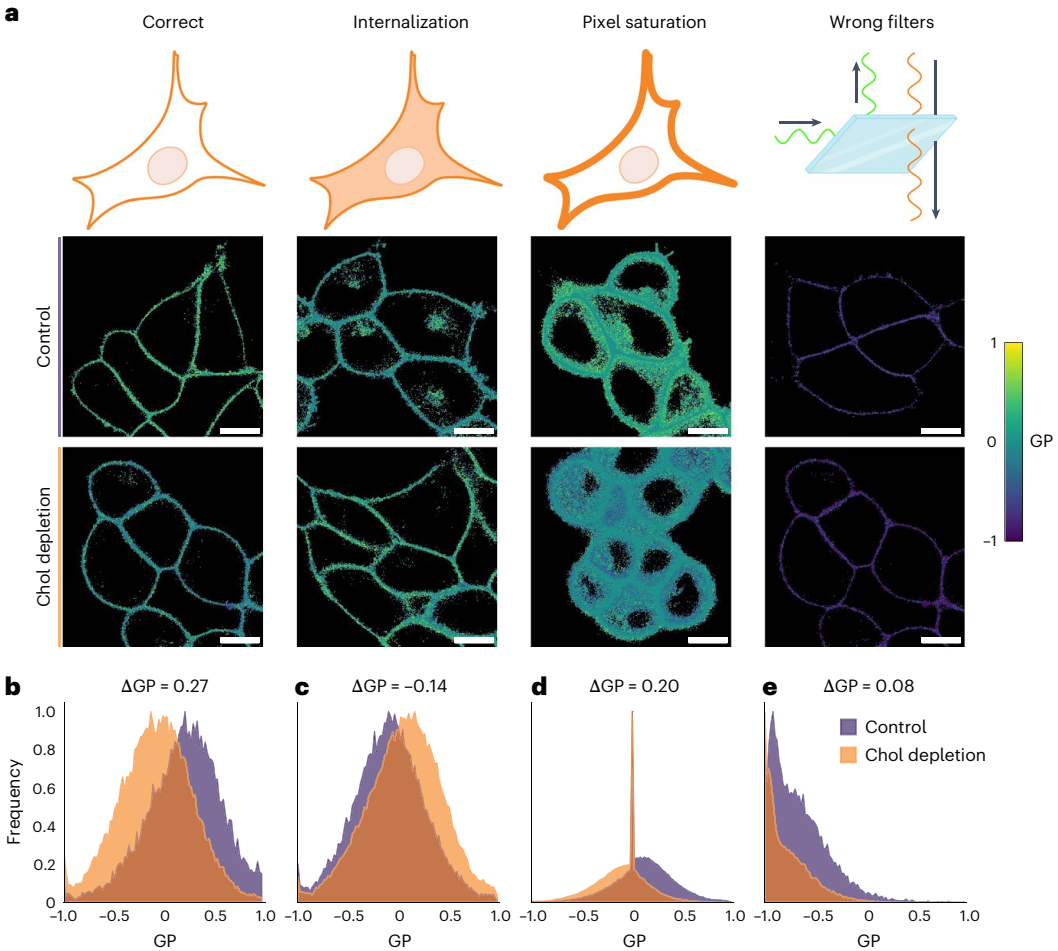

Fig. 11 | Impact of cholesterol depletion by MβCD-treatment on GP in the context of erroneous acquisition parameters. a, A schematic presentation of common errors (first row) and their impact on the final GP map before (second row) and after cholesterol depletion (third row) in HEK-293T cells upon 5 mM MβCD-treatment for 30 min in L15 medium. The cells are labeled with 300 nM NR12A after treatment. Scale bars, 20 µm. **b**–**e**, The normalized GP histogram distribution is shown for each condition of the column before and after cholesterol depletion using MβCD. Note that reliable and robust decrease of GP values caused by MβCD-treatment can only be observed when using the correct settings of the first column.

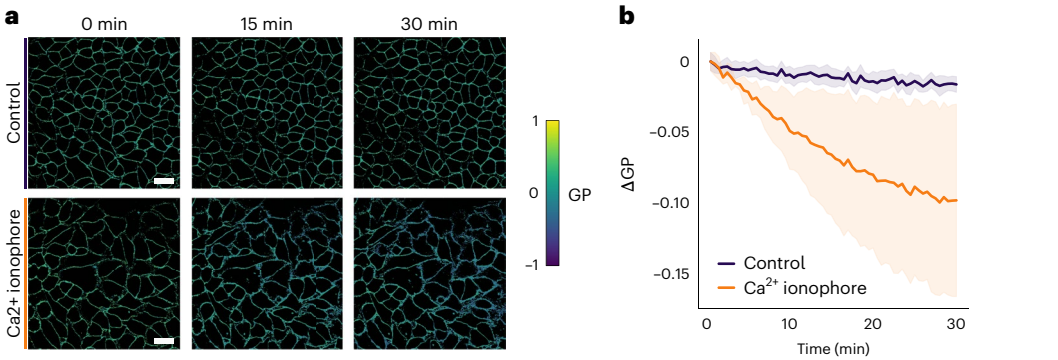

Fig. 12 | Spectral imaging of plasma membrane fluidity changes over time. a, Representative GP images at 0, 15 and 30 min of control and A23187 Ca^{2+} ionophore-treated (A23187) HeLa cells stained with 500 nM NR4A. **b**, GP change over time upon treatment with a Ca^{2+} ionophore. The lines are means and the shaded areas are standard deviations of three independent measurements. Scale bars, 20 µm.

membrane inner and outer leaflet and renders the outer leaflet more fluid[34]. NR4A, which localizes to the outer leaflet, senses this change. Figure 12b shows the GP over time in control and treated cells for the 30 min imaging period. GP does not change notably in control sample, while A23187-treated cells become more fluid over time.

Data availability

All data in this manuscript are publicly available at FigShare via https://doi.org/10.17044/scilifelab.26067604.

Code availability

The ImageJ GP plugin and representative images are available at GitHub via https://github.com/pcarravilla/fluiditycalculator/tree/main. The documentation for the data analysis tool can be found via https://github.com/pcarravilla/fluiditycalculator/wiki/Documentation.

Received: 29 April 2024; Accepted: 29 November 2024;

References

1. van Meer, G., Voelker, D. R. & Feigenson, G. W. Membrane lipids: where they are and how they behave. *Nat. Rev. Mol. Cell Biol.* **9**, 112–124 (2008).
2. Grecco, H. E., Schmick, M. & Bastiaens, P. I. H. Signaling from the living plasma membrane. *Cell* **144**, 897–909 (2011).
3. Céspedes, P. F., Beckers, D., Dustin, M. L. & Sezgin, E. Model membrane systems to reconstitute immune cell signaling. *FEBS J.* **288**, 1070–1090 (2021).
4. Ingólfsson, H. I. et al. Lipid organization of the plasma membrane. *J. Am. Chem. Soc.* **136**, 14554–14559 (2014).
5. Lorent, J. H. et al. Plasma membranes are asymmetric in lipid unsaturation, packing and protein shape. *Nat. Chem. Biol.* **16**, 644–652 (2020).
6. Harayama, T. & Riezman, H. Understanding the diversity of membrane lipid composition. *Nat. Rev. Mol. Cell Biol.* **19**, 281–296 (2018).
7. Sezgin, E., Levental, I., Mayor, S. & Eggeling, C. The mystery of membrane organization: composition, regulation and roles of lipid rafts. *Nat. Rev. Mol. Cell Biol.* **18**, 361–374 (2017).
8. Atilla-Gokcumen, G. E. et al. Dividing cells regulate their lipid composition and localization. *Cell* **156**, 428–439 (2014).
9. Kunduri, G., Acharya, U. & Acharya, J. K. Lipid polarization during cytokinesis. *Cells* **11**, 3977 (2022).
10. Lühr, J. J. et al. Maturation of monocyte-derived DCs leads to increased cellular stiffness, higher membrane fluidity, and changed lipid composition. *Front. Immunol.* **11**, 590121 (2020).
11. Miehle, F. et al. Lipidomic phenotyping reveals extensive lipid remodeling during adipogenesis in human adipocytes. *Metabolites* **10**, 217 (2020).
12. Braig, S. et al. Pharmacological targeting of membrane rigidity: implications on cancer cell migration and invasion. *N. J. Phys.* **17**, 083007 (2015).
13. Edmond, V. et al. Downregulation of ceramide synthase-6 during epithelial-to-mesenchymal transition reduces plasma membrane fluidity and cancer cell motility. *Oncogene* **34**, 996–1005 (2015).
14. Rentero, C. et al. Functional implications of plasma membrane condensation for T Cell activation. *PLoS ONE* **3**, e2262 (2008).
15. Urbančič, I. et al. Aggregation and mobility of membrane proteins interplay with local lipid order in the plasma membrane of T cells. *FEBS Lett.* **595**, 2127–2146 (2021).
16. Rudd-Schmidt, J. A. et al. Lipid order and charge protect killer T cells from accidental death. *Nat. Commun.* **10**, 5396 (2019).
17. Zhao, W. et al. Candidate antimetastasis drugs suppress the metastatic capacity of breast cancer cells by reducing membrane fluidity. *Cancer Res.* **76**, 2037–2049 (2016).
18. Goossens, P. et al. Membrane cholesterol efflux drives tumor-associated macrophage reprogramming and tumor progression. *Cell Metab.* **29**, 1376–1389.e4 (2019).
19. Powell, N., Chaudhary, S. & Zaidi, A. It is time for an oil change: polyunsaturated fatty acids and human health. *Mo. Med.* **118**, 426–430 (2021).
20. Bianchetti, G. et al. Erythrocyte membrane fluidity: a novel biomarker of residual cardiovascular risk in type 2 diabetes. *Eur. J. Clin. Invest.* **54**, e14121 (2023).
21. Niko, Y. & Klymchenko, A. S. Emerging solvatochromic push–pull dyes for monitoring the lipid order of biomembranes in live cells. *J. Biochem. (Tokyo)* **170**, 163–174 (2021).
22. Klymchenko, A. S. & Kreder, R. Fluorescent probes for lipid rafts: from model membranes to living cells. *Chem. Biol.* **21**, 97–113 (2014).
23. Jurkiewicz, P., Sýkora, J., Olżyńska, A., Humpolickova, J. & Hof, M. Solvent relaxation in phospholipid bilayers: principles and recent applications. *J. Fluoresc.* **15**, 883–894 (2005).
24. Klymchenko, A. S. Solvatochromic and fluorogenic dyes as environment-sensitive probes: design and biological applications. *Acc. Chem. Res.* **50**, 366–375 (2017).
25. Parasassi, T., De Stasio, G., d'Ubaldo, A. & Gratton, E. Phase fluctuation in phospholipid membranes revealed by Laurdan fluorescence. *Biophys. J.* **57**, 1179–1186 (1990).
26. Sezgin, E., Waithe, D., Bernardino de la Serna, J. & Eggeling, C. Spectral imaging to measure heterogeneity in membrane lipid packing. *ChemPhysChem* **16**, 1387–1394 (2015).
27. Parasassi, T., Gratton, E., Yu, W. M., Wilson, P. & Levi, M. Two-photon fluorescence microscopy of Laurdan generalized polarization domains in model and natural membranes. *Biophys. J.* **72**, 2413–2429 (1997).
28. Owen, D. M., Rentero, C., Magenau, A., Abu-Siniyeh, A. & Gaus, K. Quantitative imaging of membrane lipid order in cells and organisms. *Nat. Protoc.* **7**, 24–35 (2011).
29. Andronico, L. A. et al. High-throughput analysis of membrane fluidity unveils a hidden dimension in immune cell states. Preprint at *bioRxiv* https://doi.org/10.1101/2024.01.15.575649 (2024).
30. Dodes Traian, M. M., Gonzalez Flecha, F. L. & Levi, V. Imaging lipid lateral organization in membranes with C-laurdan in a confocal microscope. *J. Lipid Res.* **53**, 609–616 (2012).
31. Jin, L. et al. Characterization and application of a new optical probe for membrane lipid domains. *Biophys. J.* **90**, 2563–2575 (2006).
32. Aron, M. et al. Spectral imaging toolbox: segmentation, hyperstack reconstruction, and batch processing of spectral images for the determination of cell and model membrane lipid order. *BMC Bioinforma.* **18**, 254 (2017).
33. Chiantia, S., Schwille, P., Klymchenko, A. S. & London, E. Asymmetric GUVs prepared by MβCD-mediated lipid exchange: an FCS study. *Biophys. J.* **100**, L1–L3 (2011).
34. Doktorova, M. et al. Cell membranes sustain phospholipid imbalance via cholesterol asymmetry. Preprint at *bioRxiv* https://doi.org/10.1101/2023.07.30.551157 (2023).
35. Kreder, R. et al. Solvatochromic Nile Red probes with FRET quencher reveal lipid order heterogeneity in living and apoptotic cells. *ACS Chem. Biol.* **10**, 1435–1442 (2015).
36. Felce, J. et al. CD45 exclusion and cross-linking based receptor signaling together broaden FcεRI reactivity. *Sci. Signal.* **11**, eaat0756 (2018).
37. Jenkins, E. et al. Reconstitution of immune cell interactions in free-standing membranes. *J. Cell Sci.* https://doi.org/10.1242/jcs.219709 (2018).
38. Darwich, Z., Klymchenko, A. S., Dujardin, D. & Mély, Y. Imaging lipid order changes in endosome membranes of live cells by using a Nile Red-based membrane probe. *RSC Adv.* **4**, 8481–8488 (2014).
39. Iaea, D. B. & Maxfield, F. R. Membrane order in the plasma membrane and endocytic recycling compartment. *PLoS ONE* **12**, e0188041 (2017).
40. Kim, J. H., Singh, A., Del Poeta, M., Brown, D. A. & London, E. The effect of sterol structure upon clathrin-mediated and clathrin-independent endocytosis. *J. Cell Sci.* **130**, 2682–2695 (2017).
41. Sundukova, M. et al. A chemogenetic approach for the optical monitoring of voltage in neurons. *Angew. Chem.* **131**, 2363–2366 (2019).
42. Saha, S. et al. Active emulsions in living cell membranes driven by contractile stresses and transbilayer coupling. *Proc. Natl Acad. Sci.* **119**, e2123056119 (2022).
43. Plochberger, B. et al. Lipoprotein particles interact with membranes and transfer their cargo without receptors. *Biochemistry* **59**, 4421–4428 (2020).
44. Levental, K. R. et al. ω-3 polyunsaturated fatty acids direct differentiation of the membrane phenotype in mesenchymal stem cells to potentiate osteogenesis. *Sci. Adv.* **3**, eaao1193 (2017).

45. Owen, D. M. et al. High plasma membrane lipid order imaged at the immunological synapse periphery in live T cells. *Mol. Membr. Biol.* **27**, 178–189 (2010).
46. Cikes, D. et al. PCYT2-regulated lipid biosynthesis is critical to muscle health and ageing. *Nat. Metab.* **5**, 495–515 (2023).
47. Leng, H. et al. Modulating glycosphingolipid metabolism and autophagy improves outcomes in pre-clinical models of myeloma bone disease. *Nat. Commun.* **13**, 7868 (2022).
48. Matias, M. I. et al. Regulatory T cell differentiation is controlled by αKG-induced alterations in mitochondrial metabolism and lipid homeostasis. *Cell Rep.* **37**, 109911 (2021).
49. Sych, T. et al. High-throughput measurement of the content and properties of nano-sized bioparticles with single-particle profiler. *Nat. Biotechnol.* https://doi.org/10.1038/s41587-023-01825-5 (2023).
50. Sezgin, E. & Schwille, P. Fluorescence techniques to study lipid dynamics. *Cold Spring Harb. Perspect. Biol.* **3**, a009803 (2011).
51. Nguyen, T. D., Chen, Y.-I., Chen, L. H. & Yeh, H.-C. Recent advances in single-molecule tracking and imaging techniques. *Annu. Rev. Anal. Chem.* **16**, 253–284 (2023).
52. Benninger, R. K. P. Fluorescence linear dichroism imaging for quantifying membrane order. *Methods Mol. Biol. Clifton NJ* **1232**, 161–179 (2015).
53. Brasselet, S. et al. in *Fluorescent Methods to Study Biological Membranes* (eds. Mély, Y. & Duportail, G.) 311–337 (Springer, Berlin, Heidelberg, 2013); https://doi.org/10.1007/4243_2012_51
54. García-Calvo, J. et al. HydroFlipper membrane tension probes: imaging membrane hydration and mechanical compression simultaneously in living cells. *Chem. Sci.* **13**, 2086–2093 (2022).
55. Ragaller, F. et al. Quantifying fluorescence lifetime responsiveness of environment-sensitive probes for membrane fluidity measurements. *J. Phys. Chem. B* https://doi.org/10.1021/acs.jpcb.3c07006 (2024).
56. Datta, R., Heaster, T. M., Sharick, J. T., Gillette, A. A. & Skala, M. C. Fluorescence lifetime imaging microscopy: fundamentals and advances in instrumentation, analysis, and applications. *J. Biomed. Opt.* **25**, 071203 (2020).
57. Fuentes, N. R., Salinas, M. L., Wang, X., Fan, Y.-Y. & Chapkin, R. S. in *Ras Activity and Signaling: Methods and Protocols* (eds. Rubio, I. & Prior, I.) 251–258 (Springer US, New York, 2021); https://doi.org/10.1007/978-1-0716-1190-6_14
58. Rožanc, J., Finšgar, M. & Maver, U. Progressive use of multispectral imaging flow cytometry in various research areas. *Analyst* **146**, 4985–5007 (2021).
59. Fridolf, S. et al. Molecular dynamics simulations and solid-state nuclear magnetic resonance spectroscopy measurements of C–H bond order parameters and effective correlation times in a POPC–GM3 bilayer. *Phys. Chem. Chem. Phys. PCCP* **24**, 25588–25601 (2022).
60. Parkkila, P., Elderdfi, M., Bunker, A. & Viitala, T. Biophysical characterization of supported lipid bilayers using parallel dual-wavelength surface plasmon resonance and quartz crystal microbalance measurements. *Langmuir* **34**, 8081–8091 (2018).
61. Gaus, K., Zech, T. & Harder, T. Visualizing membrane microdomains by Laurdan 2-photon microscopy (review). *Mol. Membr. Biol.* **23**, 41–48 (2006).
62. Amaro, M., Reina, F., Hof, M., Eggeling, C. & Sezgin, E. Laurdan and Di-4-ANEPPDHQ probe different properties of the membrane. *J. Phys. D.* **50**, 134004 (2017).
63. Ragaller, F. et al. Dissecting the mechanisms of environment sensitivity of smart probes for quantitative assessment of membrane properties. *Open Biol.* **12**, 220175 (2022).
64. Patra, C. et al. Solvatochromic reporter to image plasma membrane order leaflet by leaflet reveals a highly asymmetric bilayer locally modulated by transbilayer interaction. Preprint at *bioRxiv* https://doi.org/10.1101/2024.07.23.604763 (2024).
65. Sezgin, E., Sadowski, T. & Simons, K. Measuring lipid packing of model and cellular membranes with environment sensitive probes. *Langmuir* **30**, 8160–8166 (2014).
66. Barucha-Kraszewska, J., Kraszewski, S., Jurkiewicz, P., Ramseyer, C. & Hof, M. Numerical studies of the membrane fluorescent dyes dynamics in ground and excited states. *Biochim. Biophys. Acta BBA* **1798**, 1724–1734 (2010).
67. Barucha-Kraszewska, J., Kraszewski, S. & Ramseyer, C. Will C-Laurdan dethrone Laurdan in fluorescent solvent relaxation techniques for lipid membrane studies? *Langmuir* **29**, 1174–1182 (2013).
68. Danylchuk, D. I., Sezgin, E., Chabert, P. & Klymchenko, A. S. Redesigning solvatochromic probe laurdan for imaging lipid order selectively in cell plasma membranes. *Anal. Chem.* **92**, 14798–14805 (2020).
69. Danylchuk, D. I., Moon, S., Xu, K. & Klymchenko, A. S. Switchable solvatochromic probes for live-cell super-resolution imaging of plasma membrane organization. *Angew. Chem.* **131**, 15062–15066 (2019).
70. Kaiser, H. J. et al. Order of lipid phases in model and plasma membranes. *Proc. Natl Acad. Sci. USA* **106**, 16645–16650 (2009).
71. Sezgin, E. et al. Partitioning, diffusion, and ligand binding of raft lipid analogs in model and cellular plasma membranes. *Biochim. Biophys. Acta* **1818**, 1777–1784 (2012).
72. Sezgin, E. et al. Adaptive lipid packing and bioactivity in membrane domains. *PLoS ONE* **10**, e0123930 (2015).
73. Sezgin, E. et al. Elucidating membrane structure and protein behavior using giant plasma membrane vesicles. *Nat. Protoc.* **7**, 1042–1051 (2012).
74. Klymchenko, A. S. Fluorescent probes for lipid membranes: from the cell surface to organelles. *Acc. Chem. Res.* **56**, 1–12 (2023).
75. Carravilla, P. et al. Long-term STED imaging of membrane packing and dynamics by exchangeable polarity-sensitive dyes. *Biophys. Rep.* **1**, 100023 (2021).
76. Sezgin, E. et al. Polarity-sensitive probes for superresolution stimulated emission depletion microscopy. *Biophys. J.* **113**, 1321–1330 (2017).
77. Amaro, M. et al. Time-resolved fluorescence in lipid bilayers: selected applications and advantages over steady state. *Biophys. J.* **107**, 2751–2760 (2014).
78. Ma, Y., Benda, A., Kwiatek, J., Owen, D. M. & Gaus, K. Time-resolved laurdan fluorescence reveals insights into membrane viscosity and hydration levels. *Biophys. J.* **115**, 1498–1508 (2018).
79. Parasassi, T., De Stasio, G., Ravagnan, G., Rusch, R. M. & Gratton, E. Quantitation of lipid phases in phospholipid vesicles by the generalized polarization of Laurdan fluorescence. *Biophys. J.* **60**, 179–189 (1991).
80. Greenspan, P. & Fowler, S. D. Spectrofluorometric studies of the lipid probe, Nile Red. *J. Lipid Res.* **26**, 781–789 (1985).
81. Greenspan, P., Mayer, E. P. & Fowler, S. D. Nile Red: a selective fluorescent stain for intracellular lipid droplets. *J. Cell Biol.* **100**, 965–973 (1985).
82. Suhaj, A., Gowland, D., Bonini, N., Owen, D. M. & Lorenz, C. D. Laurdan and di-4-ANEPPDHQ influence the properties of lipid membranes: a classical molecular dynamics and fluorescence study. *J. Phys. Chem. B* **124**, 11419–11430 (2020).
83. Dasgupta, A. et al. Effects and avoidance of photoconversion-induced artifacts in confocal and STED microscopy. *Nat. Methods* https://doi.org/10.1038/s41592-024-02297-4 (2024).
84. Bagatolli, L. A. To see or not to see: lateral organization of biological membranes and fluorescence microscopy. *Biochim. Biophys. Acta* **1758**, 1541–1556 (2006).
85. Heine, J. et al. Three dimensional live-cell STED microscopy at increased depth using a water immersion objective. *Rev. Sci. Instrum.* **89**, 053701 (2018).
86. Weber, F. et al. VISION—an open-source software for automated multi-dimensional image analysis of cellular biophysics. Preprint at *bioRxiv* https://doi.org/10.1101/2024.03.29.587344 (2024).
87. Azbazdar, Y. et al. More favorable palmitic acid over palmitoleic acid modification of wnt3 ensures its localization and activity in plasma membrane domains. *Front. Cell Dev. Biol.* **7**, 281 (2019).
88. Mahammad, S. & Parmryd, I. in *Methods in Membrane Lipids* Vol. 1232 (ed. Owen, D. M.) 91–102 (Springer New York, 2015).
89. Sanchez, S. A., Gunther, G., Tricerri, M. A. & Gratton, E. Methyl-β-cyclodextrins preferentially remove cholesterol from the liquid disordered phase in giant unilamellar vesicles. *J. Membr. Biol.* **241**, 1–10 (2011).
90. Zidovetzki, R. & Levitan, I. Use of cyclodextrins to manipulate plasma membrane cholesterol content: evidence, misconceptions and control strategies. *Biochim. Biophys. Acta* **1768**, 1311–1324 (2007).
91. Gupta, A., Korte, T., Herrmann, A. & Wohland, T. Plasma membrane asymmetry of lipid organization: fluorescence lifetime microscopy and correlation spectroscopy analysis. *J. Lipid Res.* **61**, 252–266 (2020).
92. Simbari, F. et al. Plasmalogen enrichment in exosomes secreted by a nematode parasite versus those derived from its mouse host: implications for exosome stability and biology. *J. Extracell. Vesicles* **5**, 30741 (2016).
93. Abou Karam, P. et al. Malaria parasites release vesicle subpopulations with signatures of different destinations. *EMBO Rep.* **23**, e54755 (2022).
94. Kissmann, J. et al. H1N1 influenza virus-like particles: physical degradation pathways and identification of stabilizers. *J. Pharm. Sci.* **100**, 634–645 (2011).
95. Hu, L. et al. Biophysical characterization and conformational stability of Ebola and Marburg virus-like particles. *J. Pharm. Sci.* **100**, 5156–5173 (2011).
96. Chojnacki, J. et al. Envelope glycoprotein mobility on HIV-1 particles depends on the virus maturation state. *Nat. Commun.* **8**, 545 (2017).
97. Huarte, N. et al. Functional organization of the HIV lipid envelope. *Sci. Rep.* **6**, 34190 (2016).
98. Szulczewski, J. M. et al. In vivo visualization of stromal macrophages via label-free FLIM-based metabolite imaging. *Sci. Rep.* **6**, 25086 (2016).
99. Walsh, A. J. et al. Classification of T-cell activation via autofluorescence lifetime imaging. *Nat. Biomed. Eng.* **5**, 77–88 (2021).
100. Berezin, M. Y. et al. Near-infrared fluorescence lifetime pH-Sensitive probes. *Biophys. J.* **100**, 2063–2072 (2011).
101. Maji, D. et al. Cellular trafficking of Sn-2 phosphatidylcholine prodrugs studied with fluorescence lifetime imaging and super-resolution microscopy. *Precis. Nanomed.* **1**, 128–145 (2018).
102. DUNCAN, R. R. Fluorescence lifetime imaging microscopy (FLIM) to quantify protein-protein interactions inside cells. *Biochem. Soc. Trans.* **34**, 679–682 (2006).
103. Elangovan, M., Day, R. N. & Periasamy, A. Nanosecond fluorescence resonance energy transfer-fluorescence lifetime imaging microscopy to localize the protein interactions in a single living cell. *J. Microsc.* **205**, 3–14 (2002).
104. Solomon, M. et al. Detection of enzyme activity in orthotopic murine breast cancer by fluorescence lifetime imaging using a fluorescence resonance energy transfer–based molecular probe. *J. Biomed. Opt.* **16**, 066019 (2011).
105. Golfetto, O., Hinde, E. & Gratton, E. Laurdan fluorescence lifetime discriminates cholesterol content from changes in fluidity in living cell membranes. *Biophys. J.* **104**, 1238–1247 (2013).
106. Owen, D. M. et al. Fluorescence lifetime imaging provides enhanced contrast when imaging the phase-sensitive dye di-4-ANEPPDHQ in model membranes and live cells. *Biophys. J.* **90**, L80–L82 (2006).
107. Niko, Y., Didier, P., Mely, Y., Konishi, G. & Klymchenko, A. S. Bright and photostable push-pull pyrene dye visualizes lipid order variation between plasma and intracellular membranes. *Sci. Rep.* **6**, 18870 (2016).

108. Levitt, J. A., Chung, P.-H. & Suhling, K. Spectrally resolved fluorescence lifetime imaging of Nile red for measurements of intracellular polarity. *J. Biomed. Opt.* **20**, 096002 (2015).
109. Chen, X.-X. et al. Fluorescent flippers: small-molecule probes to image membrane tension in living systems. *Angew. Chem. Int. Ed.* **62**, e202217868 (2023).
110. Colom, A. et al. A fluorescent membrane tension probe. *Nat. Chem.* **10**, 1118–1125 (2018).
111. Goujon, A. et al. Mechanosensitive fluorescent probes to image membrane tension in mitochondria, endoplasmic reticulum, and lysosomes. *J. Am. Chem. Soc.* **141**, 3380–3384 (2019).
112. López-Duarte, I., Vu, T. T., Izquierdo, M. A., Bull, J. A. & Kuimova, M. K. A molecular rotor for measuring viscosity in plasma membranes of live cells. *Chem. Commun.* **50**, 5282–5284 (2014).
113. Ashoka, A. H., Ashokkumar, P., Kovtun, Y. P. & Klymchenko, A. S. Solvatochromic near-infrared probe for polarity mapping of biomembranes and lipid droplets in cells under stress. *J. Phys. Chem. Lett.* **10**, 2414–2421 (2019).
114. Valanciunaite, J. et al. Polarity mapping of cells and embryos by improved fluorescent solvatochromic pyrene probe. *Anal. Chem.* **92**, 6512–6520 (2020).
115. Jiang, N. et al. Ratiometric fluorescence imaging of cellular polarity: decrease in mitochondrial polarity in cancer cells. *Angew. Chem. Int. Ed.* **54**, 2510–2514 (2015).
116. Liu, C., Tian, M. & Lin, W. A unique polarity-sensitive photothermal sensitizer revealing down-regulated mitochondrial polarity during photo-induced cell death. *J. Mater. Chem. B* **8**, 752–757 (2020).
117. Palacios-Serrato, E., Araiza-Olivera, D. & Jiménez-Sánchez, A. Fluorescent probe for transmembrane dynamics during osmotic effects. *Anal. Chem.* **92**, 3888–3895 (2020).
118. Guo, R., Yin, J., Ma, Y., Wang, Q. & Lin, W. A novel mitochondria-targeted rhodamine analogue for the detection of viscosity changes in living cells, zebra fish and living mice. *J. Mater. Chem. B* **6**, 2894–2900 (2018).
119. Jiménez-Sánchez, A., Lei, E. K. & Kelley, S. O. A multifunctional chemical probe for the measurement of local micropolarity and microviscosity in mitochondria. *Angew. Chem. Int. Ed.* **57**, 8891–8895 (2018).
120. Li, L.-L. et al. BODIPY-based two-photon fluorescent probe for real-time monitoring of lysosomal viscosity with fluorescence lifetime imaging microscopy. *Anal. Chem.* **90**, 5873–5878 (2018).
121. Danylchuk, D. I., Jouard, P.-H. & Klymchenko, A. S. Targeted solvatochromic fluorescent probes for imaging lipid order in organelles under oxidative and mechanical stress. *J. Am. Chem. Soc.* **143**, 912–924 (2021).
122. Chambers, J. E. et al. An optical technique for mapping microviscosity dynamics in cellular organelles. *ACS Nano* **12**, 4398–4407 (2018).
123. Straková, K. et al. HaloFlippers: a general tool for the fluorescence imaging of precisely localized membrane tension changes in living cells. *ACS Cent. Sci.* **6**, 1376–1385 (2020).
124. Pelletier, R. et al. Genetic targeting of solvatochromic dyes for probing nanoscale environments of proteins in organelles. *Anal. Chem.* **95**, 8512–8521 (2023).
125. Prifti, E. et al. A fluorogenic probe for SNAP-tagged plasma membrane proteins based on the solvatochromic molecule Nile Red. *ACS Chem. Biol.* **9**, 606–612 (2014).
126. Hanser, F. et al. Nile Red-based GPCR ligands as ultrasensitive probes of the local lipid microenvironment of the receptor. *ACS Chem. Biol.* **16**, 651–660 (2021).
127. Umebayashi, M. et al. A covalently linked probe to monitor local membrane properties surrounding plasma membrane proteins. *J. Cell Biol.* **222**, e202206119 (2022).

Acknowledgements

We thank A. Klymchenko for sharing the probes. This work is supported by Swedish Research Council Starting Grant (grant no. 2020-02682), Wellcome Leap's Dynamic Resilience Program (jointly funded by Temasek Trust), Human Frontier Science Program (RGP0025/2022) and Longevity Impetus Grant from Norn Group, Hevolution Foundation and Rosenkranz Foundation. We thank the SciLifeLab Advanced Light Microscopy facility and National Microscopy Infrastructure (VR-RFI 2016-00968) for their support on imaging.

Author contributions

P.C., J.S. and L.A contributed equally to this work. All authors contributed to manuscript writing and experiments. P.C. provided the data analysis tool.

Competing interests

The authors declare no competing interests.

Additional information

Correspondence and requests for materials should be addressed to Erdinc Sezgin.

Peer review information *Nature Protocols* thanks Mutsuo Nuriya and the other, anonymous, reviewer(s) for their contribution to the peer review of this work.

Reprints and permissions information is available at www.nature.com/reprints.

Publisher's note Springer Nature remains neutral with regard to jurisdictional claims in published maps and institutional affiliations.

Springer Nature or its licensor (e.g. a society or other partner) holds exclusive rights to this article under a publishing agreement with the author(s) or other rightsholder(s); author self-archiving of the accepted manuscript version of this article is solely governed by the terms of such publishing agreement and applicable law.

© Springer Nature Limited 2024

QUERY FORM

Manuscript ID	
Author	

AUTHOR:

The following queries have arisen during the editing of your manuscript. Please answer by making the requisite corrections directly in the e.proofing tool rather than marking them up on the PDF. This will ensure that your corrections are incorporated accurately and that your paper is published as quickly as possible.

Query No.	*Nature of Query*
Q1:	Please carefully check the spelling and numbering of all author names and affiliations.
Q2:	Please confirm the edits made to the abstract are ok.
Q3:	Please note, we reserve 'significant' and its derivatives for statistical significance. Please reword where this is not the intended meaning (for example to important, notable, substantial); there are 10 instances throughout your text.
Q4:	Please confirm the edits made to the introduction are ok.
Q5:	Please confirm the edits have retained the intended meaning.
Q6:	Please check your article carefully, coordinate with any co-authors and enter all final edits clearly in the eproof, remembering to save frequently. Once corrections are submitted, we cannot routinely make further changes to the article.
Q7:	Note that the eproof should be amended in only one browser window at any one time; otherwise changes will be overwritten.
Q8:	Author surnames have been highlighted. Please check these carefully and adjust if the first name or surname is marked up incorrectly, as this will affect indexing of your article in public repositories such as PubMed. Also, carefully check the spelling and numbering of all author names and affiliations, and the corresponding author(s) email address(es). Please note that email addresses should only be included for designated corresponding authors, and you cannot change corresponding authors at this stage except to correct errors made during typesetting.
Q9:	Please check Figures for accuracy as they have been relabelled. Please markup minor changes in the eProof. For major changes, please provide revised figures. (Please note that in the eProof the figure resolution will appear at lower resolution than in the pdf and html versions of your paper.)
Q10:	Please carefully check all the step numbers throughout the manuscript (text and figures) as some may have been renumbered.

Uncorrected proofs

QUERY FORM

Manuscript ID	
Author	

AUTHOR:

The following queries have arisen during the editing of your manuscript. Please answer by making the requisite corrections directly in the e.proofing tool rather than marking them up on the PDF. This will ensure that your corrections are incorporated accurately and that your paper is published as quickly as possible.

Query No.	*Nature of Query*
Q11:	Please confirm the edits have retained the intended meaning:.
Q12:	In Fig. 1 caption, please define 'Int.'.
Q13:	Please expand 'GPI'.
Q14:	Original Reference [15 with 46,50 with 100,66 with 81 and 57 with 101] is a duplicate of [46,100,81 and 101] and hence the repeated version has been deleted. Please check.
Q15:	Please expand 'GPCR'.
Q16:	Please expand 'GPI',.
Q17:	In Fig. 3 caption, please define 'norm.'.
Q18:	In Fig. 4 caption, please define 'Sat.'.
Q19:	Please define 'Chol', if applicable.
Q20:	In Fig. 8 caption, please define 'norm.'.
Q21:	Please confirm the edits have retained the intended meaning;.
Q22:	In Fig. 9 caption, please clarify the difference between panels b–e. In panel b, please define 'norm.'.
Q23:	Please confirm the edits made to the materials are ok.
Q24:	Please check the protocol thoroughly to make sure that all materials mentioned are listed in the Materials section, along with supplier and catalog/model number. This will help to ensure that readers can successfully use your protocol.

Uncorrected proofs

QUERY FORM

Manuscript ID	
Author	

AUTHOR:

The following queries have arisen during the editing of your manuscript. Please answer by making the requisite corrections directly in the e.proofing tool rather than marking them up on the PDF. This will ensure that your corrections are incorporated accurately and that your paper is published as quickly as possible.

Query No.	*Nature of Query*
Q25:	Per journal requirements, all items listed in the "Reagents" and "Equipment" sections (aside from materials such as regular water that would not be obtained from an outside supplier) should include the supplier name and catalog and/or model number, or citation of a protocol for obtaining the material. Please check the lists carefully and add this information where applicable.
Q26:	Please provide the supplier and cat. no.
Q27:	Please provide the supplier and cat no.
Q28:	Please provide the supplier and cat., no.
Q29:	Please provide the cat. no,.
Q30:	Please provide the cat,. no.
Q31:	Please provide the, cat. no.
Q32:	Please confirm the edits made to the procedure are ok.
Q33:	Please define room temperature.
Q34:	Please define 'TIFF' and 'CSV'.
Q35:	Please confirm the edits made to the troubleshooting are ok.
Q36:	Please confirm the edits made to the timing are ok.
Q37:	Please confirm the edits have retained, the intended meaning.
Q38:	Please confirm the edits made to the anticipated results are ok.
Q39:	Please confirm the edits made to the data availability are ok.

Uncorrected Proofs

QUERY FORM

Manuscript ID	
Author	

AUTHOR:

The following queries have arisen during the editing of your manuscript. Please answer by making the requisite corrections directly in the e.proofing tool rather than marking them up on the PDF. This will ensure that your corrections are incorporated accurately and that your paper is published as quickly as possible.

Query No.	*Nature of Query*
Q40:	Please confirm the edits made to the code availability are ok.
Q41:	Please check that all funders have been appropriately acknowledged and that all grant numbers are correct.
Q42:	The References section has been moved to after the ack section, as per the journal's guidelines for protocols.
Q43:	Please check that the Competing interests statement is correct and complete.
Q44:	Please confirm the edits made to the references are ok.
Q45:	If refs. 29, 34, 64, and 86 (preprint) have now been published in final peer-reviewed form, please update the reference details if appropriate.
Q46:	If ref. 29 (preprint) has now been published in final peer-reviewed form, please update the reference details if appropriate.
Q47:	For ref. 32, please add the final page number or confirm that it is a single-page reference.
Q48:	If ref. 34 (preprint) has now been published in final peer-reviewed form, please update the reference details if appropriate.
Q49:	If ref. 64 (preprint) has now been published in final peer-reviewed form, please update the reference details if appropriate.
Q50:	If ref. 86 (preprint) has now been published in final peer-reviewed form, please update the reference details if appropriate.
Q51:	Figures are not in sequential order in the article. Please confirm if it is ok to proceed with the order provided.

Uncorrected proofs